Eur. Phys. J. D **40**, 281–296 (2006)
DOI: 10.1140/epjd/e2006-00164-5

THE EUROPEAN PHYSICAL JOURNAL D

Cross phase modulation in a five–level atomic medium: semiclassical theory

C. Ottaviani[a], S. Rebić[b], D. Vitali, and P. Tombesi

Dipartimento di Fisica Università di Camerino, 62032 Camerino, Italy

Received 14 April 2006 / Received in final form 16 June 2006
Published online 12 July 2006 –

Abstract. The interaction of a five-level atomic system involving electromagnetically induced transparency with four light fields is investigated. Two different light-atom configurations are considered, and their efficiency in generating large nonlinear cross-phase shifts compared. The dispersive properties of those schemes are analyzed in detail, and the conditions leading to group velocity matching for two of the light fields are identified. An analytical treatment based on amplitude equations is used in order to obtain approximate solutions for the susceptibilities, which are shown to fit well with the numerical solution of the full Bloch equations in a large parameter region.

PACS. 42.50.Gy Effects of atomic coherence on propagation, absorption, and amplification of light; electromagnetically induced transparency and absorption – 42.65.-k Nonlinear optics – 03.67.Hk Quantum communication

1 Introduction

An efficient cross-phase modulation (XPM) in quantum and semiclassical regimes is both interesting and useful in many possible applications, such as those in optical communications [1], optical Kerr shutters [2], quantum nondemolition measurements [3] and quantum phase gates [4]. In all of these, but the last two especially, a large XPM is desirable for low pump powers and high sensitivities.

In a standard three-level cascade scheme, shown in Figure 1b, nonlinear effects are obtained alongside absorption, which increase as the fields are tuned closer to the atomic transition [5]. To reduce the absorption to an acceptable level, light fields need to be strongly detuned from the intermediate atomic level $|2\rangle$, simultaneously reducing however the size of the nonlinearity, since both are inversely proportional to the square of the detuning.

Extensive studies aimed at avoiding this problem have been performed in recent years. A promising candidate emerged with the use of quantum coherence effects in the interaction of light with multilevel atoms. Coherent population trapping (CPT) [6] and in particular the related effect of electromagnetically induced transparency (EIT) [7,8] have been studied theoretically [5,9,10] and experimentally [3,11–13] in various energy-level schemes based on a generic Λ-scheme (see Fig. 1a). At resonance ($\delta_1 = 0$ in Fig. 1a), the presence of the coupling field (with Rabi frequency Ω_2) cancels, by destructive interference, the absorption on the probe transition (with Rabi frequency Ω_1), and renders the medium transparent for the probe beam. A more general condition for EIT is two-photon resonance, a condition that is satisfied when the frequency difference between the fields matches the energy gap between levels $|1\rangle$ and $|3\rangle$. However, on the exact EIT resonance, probe field decouples from the atoms, making the dynamics purely linear.

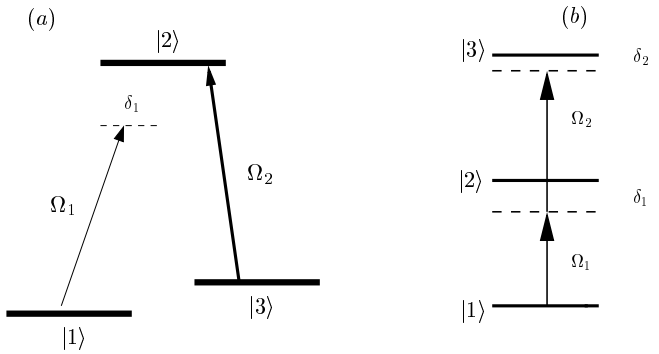

Fig. 1. (a) Three-level Λ–scheme for EIT. Transitions are driven by the probe and coupling fields, with Rabi frequency Ω_1 and Ω_2 respectively. When the probe detuning δ_1 matches the two photon Raman-resonance condition with the coupling field, the atomic medium becomes transparent for the probe field. (b) Three-level cascade configuration. To obtain significant nonlinear effects for the probe field with Rabi frequency Ω_1, a large detuning δ_1 from the intermediate level $|2\rangle$ is necessary.

[a] e-mail: carlo.ottaviani@unicam.it
[b] e-mail: stojan.rebic@unicam.it

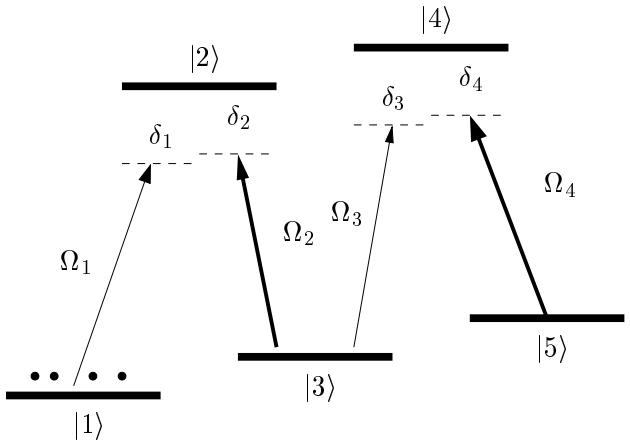

Fig. 2. Asymmetric M scheme. The probe and the trigger fields, with Rabi frequencies Ω_1 and Ω_3 respectively, together with the stronger pump fields, the coupler and the tuner (with Rabi frequencies Ω_2 and Ω_4, respectively) drive the corresponding transitions. All the atoms are assumed to be in state $|1\rangle$ and the detunings are defined in equations (3).

Optical nonlinearities in a multilevel atomic or molecular system in the presence of EIT, usually arise by one of the two following related mechanisms. One is to violate the strict two-photon resonance condition, with a frequency mismatch smaller than the width of the transparency window [3,14,15]. Alternatively, one can add additional energy level(s) in order to induce an ac-Stark shift and effectively tune the signal out of resonance [5,10,16]. Both mechanisms result in large nonlinearities, accompanied by very weak absorption. Recently, the so-called M-scheme, shown in Figure 2, has been studied and proposed as a promising source of giant nonlinearities that can be utilized for XPM [14,17]. The double Λ nature of this M configuration offers the opportunity of a simultaneous group velocity reduction for pulses propagating inside the atomic sample. Group velocity matching, originally pointed out by Lukin and Imamoğlu [18], is important to obtain a large XPM. In fact, it has been shown by Harris and Hau [10] that if equal group velocity reduction is not achieved for both fields, the nonlinear phase accumulation will saturate at a certain constant value. The consequence is that increasing the length of the sample in which the nonlinear interaction takes place is not useful. On the other hand, if group velocities are equal, the nonlinear phase accumulation becomes linear in the interaction length [18] and it may become very large.

A large cross Kerr phase shift is very useful for photonic-based implementations of quantum information (QI) processing systems [4,19]. In fact, a fundamental building block for quantum information processing is the quantum phase gate (QPG). In a QPG, one qubit gets a phase conditional to the other qubit state according to the transformation [4,20] $|i\rangle_1|j\rangle_2 \rightarrow \exp\{i\phi_{ij}\}|i\rangle_1|j\rangle_2$ where $\{i,j\} = 0,1$ denote the logical qubit bases. This gate is universal when the conditional phase shift (CPS)

$$\phi = \phi_{11} + \phi_{00} - \phi_{10} - \phi_{01}, \tag{1}$$

is nonzero, and it is equivalent to a CNOT gate up to local unitary transformations when $\phi = \pi$ [4,20].

To obtain a CPS of $\phi = \pi$, one looks for a strong interaction between qubits, ideally accompanied by weak decoherence. Photons are a particularly attractive choice for qubits due to their robustness against decoherence during the processing and transmission of information. This feature should ideally permit the transmission of the quantum information stored in very weak quantum pulses over very long distances with a negligibly small reduction of the initial signal. There is however an important difficulty in the implementation of an all–optical–QPG: to process the information one needs strong photon–photon interaction. In fact, to implement QI with photons, a nonlinear interaction is needed either to build a two-photon gate operation [14,15,21,22] or at the detection stage in linear optics quantum computation [23]. It should also be mentioned that the generation of single-photons (which is also necessary in linear optics quantum computation) also relies on nonlinear interactions.

In this paper we perform a semiclassical analysis of the interaction of light with atoms in the M configuration, in which the amplitude of the four fields involved is described in terms of the corresponding Rabi frequency. The aim is to estimate the effects of collisional dephasing and spontaneous emission, both on the nonlinear interaction and on group velocity matching. The semiclassical regime offers a clear picture of the physical aspects involved in EIT-based nonlinear optics, and well describes a number of recent experiments [13,24]. To this end we consider two different configurations of atom-field interactions, which we will call the *asymmetric* (see Fig. 2) and the *symmetric* (see Fig. 10) M scheme. The paper is thus composed of two main parts. In Section 2 we describe the physics of the asymmetric M-scheme. We start by defining the system and calculating the susceptibilities using an approximate treatment employing amplitude equations. These analytical calculations are then compared with the results of the numerical solution of the full system of Bloch equations. Finally, the conditions for group velocity matching are analyzed. In Section 3 the physics of the symmetric M-scheme is described by following the same order as in Section 2. Conclusions are drawn in Section 4.

2 The asymmetric M scheme

2.1 The system

The M-system under consideration has a double adjacent Λ structure as shown in Figure 2, where atoms with five levels (three ground states $|1\rangle$, $|3\rangle$, $|5\rangle$, and two excited states $|2\rangle$, $|4\rangle$) interact with four electromagnetic fields. This configuration can be realized in Zeeman-splitted alkali atoms, such as ^{87}Rb atoms. The Rabi frequencies associated with the lasers driving the atomic transitions are defined as

$$\Omega_k = -\frac{\mu_{ij}\mathcal{E}_k}{\hbar}, \tag{2}$$

where $\mathcal{E}_k$ is the electric field amplitude, μ_{ij} is the relative dipole matrix elements induced on the transition $|i\rangle \leftrightarrow |j\rangle$. On transitions $|3\rangle \leftrightarrow |2\rangle$ and $|5\rangle \leftrightarrow |4\rangle$ we apply two strong fields, the *coupler* Ω_2 and the *tuner* Ω_4 respectively. On the transition $|1\rangle \leftrightarrow |2\rangle$ a *probe* field is applied (with Ω_1), while on the transition $|3\rangle \leftrightarrow |4\rangle$ a *trigger* field (with Ω_3) is applied. In this paper, we will analyze the XPM and the group velocity matching between the *probe* and the *trigger* fields. We call the scheme of Figure 2 the *asymmetric M* scheme due to the asymmetric distribution of the initial atomic population. All the atoms are in fact assumed to be initially in state $|1\rangle$ so that they directly feel the effect of the probe field only, while the effect of the trigger field is only indirect. Due to this inherent asymmetry, the dynamics experienced by probe and trigger fields are always different, even when the corresponding parameters (Rabi frequencies, decay rates, detunings) are equal. The symmetric version of this scheme will be analyzed in Section 3.

The detunings δ_i (see Fig. 2) are defined as follows

$$E_2 - E_1 = \hbar\omega_1 + \hbar\delta_1 \tag{3a}$$
$$E_2 - E_3 = \hbar\omega_2 + \hbar\delta_2 \tag{3b}$$
$$E_4 - E_3 = \hbar\omega_3 + \hbar\delta_3 \tag{3c}$$
$$E_4 - E_5 = \hbar\omega_4 + \hbar\delta_4, \tag{3d}$$

where E_i, $(i = 1, \ldots, 5)$ is the energy of level $|i\rangle$, and ω_i is the frequency of the field with Rabi frequency Ω_i.

The Hamiltonian of the system is

$$H_A = \sum_i^5 E_i|i\rangle\langle i| + \hbar\left(\Omega_1 e^{-i\omega_1 t}|2\rangle\langle 1| + \Omega_2 e^{-i\omega_2 t}|2\rangle\langle 3| + \Omega_3 e^{-i\omega_3 t}|4\rangle\langle 3| + \Omega_4 e^{-i\omega_4 t}|4\rangle\langle 5| + h.c.\right), \tag{4}$$

where *h.c.* denotes the Hermitian conjugate. Moving to the interaction picture with respect to the following free Hamiltonian

$$H_0 = E_1|1\rangle\langle 1| + (E_2 - \hbar\delta_1)|2\rangle\langle 2| + (E_3 - \hbar\delta_{12})|3\rangle\langle 3| + (E_4 - \hbar\delta_{13})|4\rangle\langle 4| + (E_5 - \hbar\delta_{14})|5\rangle\langle 5|, \tag{5}$$

where

$$\delta_{12} = \delta_1 - \delta_2, \tag{6a}$$
$$\delta_{13} = \delta_1 - \delta_2 + \delta_3, \tag{6b}$$
$$\delta_{14} = \delta_1 - \delta_2 + \delta_3 - \delta_4, \tag{6c}$$

we get the following effective Hamiltonian

$$H_{eff}^{AS} = \hbar\delta_1|2\rangle\langle 2| + \hbar\delta_{12}|3\rangle\langle 3| + \hbar\delta_{13}|4\rangle\langle 4| + \hbar\delta_{14}|5\rangle\langle 5| + \hbar\Omega_1|2\rangle\langle 1| + \hbar\Omega_2|2\rangle\langle 3| + \hbar\Omega_3|4\rangle\langle 3| + \hbar\Omega_4|4\rangle\langle 5| + \hbar\Omega_1^\star|1\rangle\langle 2| + \hbar\Omega_2^\star|3\rangle\langle 2| + \hbar\Omega_3^\star|3\rangle\langle 4| + \hbar\Omega_4^\star|5\rangle\langle 4|. \tag{7}$$

2.2 Amplitude variables approach

We now study the dynamics driven by equation (7). However, we have to include the effects of spontaneous emission and dephasing, and we first treat them in a phenomenological manner by including decay rates Γ_i^{AV} for each atomic level $|i\rangle$ in the equations for the amplitude variables (AV) of the atomic wave-function. From an intuitive point of view, for the excited levels $|2\rangle$ and $|4\rangle$ these rates describe the total spontaneous decay rates, while for the ground states the associated decay rates describe dephasing processes [8]. Therefore, the evolution equations for the amplitudes $b_i(t)$ of the atomic state

$$|\psi(t)\rangle = \sum_{i=1}^{5} b_i(t)|i\rangle \tag{8}$$

become

$$\dot{b}_1 = -\frac{\Gamma_1^{AV}}{2}b_1 - i\Omega_1^\star b_2, \tag{9a}$$
$$\dot{b}_2 = -\left(\frac{\Gamma_2^{AV}}{2} + i\delta_1\right)b_2 - i\Omega_1 b_1 - i\Omega_2 b_3, \tag{9b}$$
$$\dot{b}_3 = -\left(\frac{\Gamma_3^{AV}}{2} + i\delta_{12}\right)b_3 - i\Omega_2^\star b_2 - i\Omega_3^\star b_4, \tag{9c}$$
$$\dot{b}_4 = -\left(\frac{\Gamma_4^{AV}}{2} + i\delta_{13}\right)b_4 - i\Omega_3 b_3 - i\Omega_4 b_5, \tag{9d}$$
$$\dot{b}_5 = -\left(\frac{\Gamma_5^{AV}}{2} + i\delta_{14}\right)b_5 - i\Omega_4^\star b_4. \tag{9e}$$

The system's initial state is assumed to be the ground state $|1\rangle$. Since an efficient XPM requires a dispersive interaction, we tailor the dynamics in such a way that this initial condition on the populations remains essentially unaltered, even when the system reaches the steady-state, i.e.,

$$b_1^{ss} \simeq 1. \tag{10}$$

To this end we assume that the control field Ω_2 is stronger then the probe field Ω_1, with the system being approximately on Raman resonance for the first and the second Λ subsystems ($\delta_1 \sim \delta_2$ and $\delta_3 \sim \delta_4$), equations (9) are then solved in the steady-state. In order to get a consistent expression for the nonlinear susceptibilities one has to consider higher order contributions to equation (10), which is obtained by imposing the normalization of the atomic wave-function of equation (8) at second order in $|\Omega_1/\Omega_2|$. One gets the following expression for the steady state amplitudes

$$b_1^{ss} = 1 - \frac{|\Omega_1|^2\left[|d_3|^2 + |\Omega_2|^2\right]}{2\left|d_2 d_3 - |\Omega_2|^2\right|^2}, \tag{11a}$$
$$b_2^{ss} = \Omega_1 \frac{d_3\left[|\Omega_4|^2 - d_4 d_5\right] + |\Omega_3|^2 d_5}{D_a} b_1^{ss} \tag{11b}$$
$$b_3^{ss} = -\Omega_1\Omega_2^\star \frac{|\Omega_4|^2 - d_4 d_5}{D_a} b_1^{ss} \tag{11c}$$
$$b_4^{ss} = -\frac{\Omega_1\Omega_2^\star\Omega_3 d_5}{D_a} b_1^{ss} \tag{11d}$$
$$b_5^{ss} = \frac{\Omega_1\Omega_2^\star\Omega_3\Omega_4^\star}{D_a} b_1^{ss}, \tag{11e}$$

$$\chi_P^{(3,sk)} = \frac{N|\mu_{12}|^4}{V\hbar^3\varepsilon_0} \frac{-\left(\delta_{12}-i\Gamma_3^{AV}/2\right)\left[\left|\delta_{12}-i\Gamma_3^{AV}/2\right|^2+|\Omega_2|^2\right]}{\left[\left(\delta_1-i\Gamma_2^{AV}/2\right)\left(\delta_{12}-i\Gamma_3^{AV}/2\right)-|\Omega_2|^2\right]\left|\left(\delta_1-i\Gamma_2^{AV}/2\right)\left(\delta_{12}-i\Gamma_3^{AV}/2\right)-|\Omega_2|^2\right|^2}, \tag{17a}$$

$$\chi_P^{(3,ck)} = \frac{N|\mu_{12}|^2|\mu_{34}|^2}{V\hbar^3\varepsilon_0} \frac{|\Omega_2|^2\left(\delta_{14}-i\Gamma_5^{AV}/2\right)}{\left[\left(\delta_1-i\Gamma_2^{AV}/2\right)\left(\delta_{12}-i\Gamma_3^{AV}/2\right)-|\Omega_2|^2\right]^2\left[\left(\delta_{13}-i\Gamma_4^{AV}/2\right)\left(\delta_{14}-i\Gamma_5^{AV}/2\right)-|\Omega_4|^2\right]}, \tag{17b}$$

$$\chi_T^{(3,ck)} = \frac{N|\mu_{12}|^2|\mu_{34}|^2}{V\hbar^3\varepsilon_0} \frac{|\Omega_2|^2\left(\delta_{14}-i\Gamma_5^{AV}/2\right)}{\left|\left(\delta_1-i\Gamma_2^{AV}/2\right)\left(\delta_{12}-i\Gamma_3^{AV}/2\right)-|\Omega_2|^2\right|^2\left[\left(\delta_{13}-i\Gamma_4^{AV}/2\right)\left(\delta_{14}-i\Gamma_5^{AV}/2\right)-|\Omega_4|^2\right]}, \tag{17c}$$

where we have defined

$$d_2 = \delta_1 - \imath\Gamma_2^{AV}/2, \tag{12a}$$

$$d_3 = \delta_{12} - \imath\Gamma_3^{AV}/2, \tag{12b}$$

$$d_4 = \delta_{13} - \imath\Gamma_4^{AV}/2, \tag{12c}$$

$$d_5 = \delta_{14} - \imath\Gamma_5^{AV}/2, \tag{12d}$$

$$D_a = \left[d_2d_3-|\Omega_2|^2\right]\left[d_4d_5-|\Omega_4|^2\right]-d_2d_5|\Omega_3|^2. \tag{13}$$

These results can be used to determine the probe and trigger susceptibilities, which are defined as

$$\chi_P = \frac{N\mu_{12}}{V\varepsilon_0\mathcal{E}_1}b_2^{ss}b_1^{ss,\star} = -\frac{N|\mu_{12}|^2}{V\hbar\varepsilon_0\Omega_1}b_2^{ss}b_1^{ss,\star}, \tag{14a}$$

$$\chi_T = \frac{N\mu_{34}}{V\varepsilon_0\mathcal{E}_3}b_4^{ss}b_3^{ss,\star} = -\frac{N|\mu_{34}|^2}{V\hbar\varepsilon_0\Omega_3}b_4^{ss}b_3^{ss,\star}, \tag{14b}$$

where N is the number of atoms interacting with the electromagnetic field, V is the volume occupied by the gas, and ε_0 is the vacuum dielectric constant. Doppler broadening is neglected here. It is well-known that first order Doppler effect can be cancelled by using co-propagating laser fields [6]. In particular we emphasize that this is valid for cold atomic media in a magneto-optical trap as well as for a standard gas cell.

Inserting equations (11) into equations (14) and expanding in series at the lowest orders in the probe and trigger electric fields, $\mathcal{E}_1$ and $\mathcal{E}_3$ respectively, one gets

$$\chi_P \simeq \chi_P^{(1)} + \chi_P^{(3,sk)}|\mathcal{E}_1|^2 + \chi_P^{(3,ck)}|\mathcal{E}_3|^2 \tag{15a}$$

$$\chi_T \simeq \chi_T^{(3,ck)}|\mathcal{E}_1|^2, \tag{15b}$$

where we have introduced the linear susceptibility $\chi_P^{(1)}$, the third-order self-Kerr susceptibility $\chi_P^{(3,sk)}$ and the third-order cross-Kerr susceptibilities $\chi_{P,T}^{(3,ck)}$. Equations (15) clearly show the asymmetry of the scheme between the probe and trigger fields, with the latter possessing a nonzero cross-Kerr susceptibility only. This is a consequence of the asymmetry of the population distribution, which essentially remains in the ground state $|1\rangle$ all the time. This means that the trigger field drives a virtually empty transition, hence the contribution to the susceptibility comes only from higher order (see [15] for discussion on the link between the population distribution and a linear contribution to susceptibility). It will be shown in Section 3 that the symmetric M-scheme brings about both a linear and a self-Kerr contribution to the trigger susceptibility.

By using equations (11) and the definitions of equations (12) into equations (14), and comparing with equations (15) at the corresponding order in the electric fields, one gets the explicit dependence of the linear and nonlinear susceptibilities as a function of the system parameters, i.e.,

$$\chi_P^{(1)} = \frac{N|\mu_{12}|^2}{V\hbar\varepsilon_0}\frac{\delta_{12}-i\Gamma_3^{AV}/2}{\left(\delta_1-i\Gamma_2^{AV}/2\right)\left(\delta_{12}-i\Gamma_3^{AV}/2\right)-|\Omega_2|^2} \tag{16}$$

for the probe linear susceptibility, and

see equations (17) above

for the third-order nonlinear susceptibilities. The two cross-Kerr susceptibilities are identical whenever the quantity $\left(\delta_1-i\Gamma_2^{AV}/2\right)\left(\delta_{12}-i\Gamma_3^{AV}/2\right)-|\Omega_2|^2$ is (at least approximately) real. This happens in the typical EIT situation we are considering in which $|\Omega_2|$ is large enough. In fact, when $|\Omega_2|^2 \gg \left|\left(\delta_1-i\Gamma_2^{AV}/2\right)\left(\delta_{12}-i\Gamma_3^{AV}/2\right)\right|$, one has [14]

$$\chi_P^{(3,ck)} = \chi_T^{(3,ck)} = \frac{N|\mu_{12}|^2|\mu_{34}|^2}{V\hbar^3\varepsilon_0} \times \frac{\delta_{14}-i\Gamma_5^{AV}/2}{|\Omega_2|^2\left[\left(\delta_{13}-i\Gamma_4^{AV}/2\right)\left(\delta_{14}-i\Gamma_5^{AV}/2\right)-|\Omega_4|^2\right]}. \tag{18}$$

We shall see in the next subsection that these approximate expressions for the nonlinear susceptibilities fit very well with the numerical solution of the exact dynamics of the system.

The asymmetric M-scheme can be seen as an extension of the four level N-scheme introduced in reference [5], with the addition of the coupling to an additional level $|5\rangle$ provided by the tuner field with Rabi frequency Ω_4. In fact, it is easy to check that upon setting $\Omega_4 = 0$ in equation (17b), one recovers the third-order nonlinear susceptibility of the four-level N-scheme derived in references [5,13]. As we will see below, the role of the tuner field is to enable a fine tuning of the group velocities, in order to achieve group velocity matching between probe and trigger [14,16,18].

2.3 Comparison with the optical Bloch equations

We now study the dynamics of the asymmetric M scheme of Figure 2 by means of the optical Bloch equations (OBE), which allow to describe spontaneous emission and dephasing rigorously and no more phenomenologically as in the AV treatment presented in the preceding subsection. We consider six spontaneous decay channels, i.e., the decay of the excited state $|2\rangle$ onto the three ground state sublevels $|1\rangle$, $|3\rangle$, and $|5\rangle$ with rates Γ_{21}, Γ_{23} and Γ_{25} respectively, and the corresponding decay of the excited state $|4\rangle$ onto the three sublevels $|1\rangle$, $|3\rangle$, and $|5\rangle$ with rates Γ_{41}, Γ_{43} and Γ_{45} respectively. Moreover we consider dephasing of the each level $|i\rangle$ with dephasing rate γ_{ii}, so that the master equation for the atomic density operator ρ is given by

$$\begin{aligned}\dot{\rho} = &-\frac{i}{\hbar}\left[H_{eff}^{AS},\rho\right] \\ &+\sum_{l=2,4}\sum_{k=1,3,5}\frac{\Gamma_{lk}}{2}\left(2\hat{\sigma}_{kl}\rho\hat{\sigma}_{kl}^{\dagger}-\hat{\sigma}_{kl}^{\dagger}\hat{\sigma}_{kl}\rho-\rho\hat{\sigma}_{kl}^{\dagger}\hat{\sigma}_{kl}\right) \\ &+\sum_{k=1}^{5}\frac{\gamma_{kk}}{2}\left(2\hat{\sigma}_{kk}\rho\hat{\sigma}_{kk}-\hat{\sigma}_{kk}\rho-\rho\hat{\sigma}_{kk}\right), \qquad (19)\end{aligned}$$

where H_{eff}^{AS} is given by equation (7) and $\hat{\sigma}_{kl} = |k\rangle\langle l|$. The corresponding system of OBE's for the mean values $\sigma_{ij}(t) \equiv \langle\hat{\sigma}_{ij}(t)\rangle \equiv \rho_{ji}(t)$ is displayed in Appendix A as equations (A.1) and (A.2), where we have defined for convenience the total decay rates

$$\Gamma_2 = \Gamma_{21} + \Gamma_{23} + \Gamma_{25}, \qquad (20)$$

$$\Gamma_4 = \Gamma_{41} + \Gamma_{43} + \Gamma_{45}, \qquad (21)$$

and the composite dephasing rates

$$\gamma_{ij} = \gamma_{ii} + \gamma_{jj}, \quad i = 1\ldots5. \qquad (22)$$

The OBE for the M scheme are quite involved and less suited for an approximate analytical treatment with respect to the AV equations of the preceding subsection. In fact, if we consider again the condition $|\Omega_1/\Omega_2| \ll 1$ and, consistently with equation (10), we assume that

$$\sigma_{11} \approx 1, \qquad (23a)$$

$$\sigma_{jj} \approx 0, \quad j = 2,\ldots,5, \qquad (23b)$$

at the steady state, it is possible to see that by inserting equations (23) into equations (A.2) for the coherences, one gets a satisfactory expression for the probe linear susceptibility only. To be more specific, only the approximate linear susceptibility fits well with the numerical solution of the OBE, while it turns out to be extremely difficult to derive analytical expressions from equations (A.1) and (A.2) for the nonlinear susceptibilities, as simple as those of equations (17), and which reproduce in the same way the exact numerical solution in the EIT regime we are studying. Obviously, one can exactly solve analytically the OBE, but the resulting expressions are very cumbersome and not physically transparent such as those of equations (17). For this reason we will analytically derive from the OBE the probe linear susceptibility only, and we will then use the OBE only for the numerical determination of the atomic steady state. Additionally, deriving this result will enable us to draw a formal analogy between the AV and OBE treatments (see Eqs. (26) below).

The probe susceptibility is defined in terms of the atomic coherence σ_{12} as (see also Eq. (14a))

$$\chi_P = \frac{N\mu_{12}}{V\varepsilon_0\mathcal{E}_1}\sigma_{12} = -\frac{N|\mu_{12}|^2}{V\hbar\varepsilon_0\Omega_1}\sigma_{12}. \qquad (24)$$

Using equations (23) and performing a series expansion at the lowest order in the probe and trigger fields, we arrive at an approximate solution for σ_{12}, which, inserted into equation (24), gives the following expression for the probe linear susceptibility

$$\chi_P^{(1)} = \frac{N|\mu_{12}|^2}{V\hbar\varepsilon_0}\frac{\delta_{12} - i\gamma_{13}/2}{\left[\delta_{12} - i\gamma_{13}/2\right]\left[\delta_1 - i\left(\Gamma_2+\gamma_{12}\right)/2\right] - |\Omega_2|^2}. \qquad (25)$$

By comparing equation (25) with equation (16), one can immediately see that the AV and OBE predictions for the probe linear susceptibility coincide provided that the phenomenological decay rates Γ_i^{AV} are appropriately interpreted, i.e.,

$$\Gamma_2^{AV} \leftrightarrow \Gamma_2 + \gamma_{12}, \qquad (26a)$$

$$\Gamma_3^{AV} \leftrightarrow \gamma_{13}. \qquad (26b)$$

This comparison shows therefore that the AV approach provides a treatment of the atomic dynamics simpler than the OBE's approach, but roughly equivalent, and that the intuitive interpretation of its phenomenological decay rates Γ_i^{AV} as spontaneous emission total decay rates for the excited states, and as dephasing rates in the case of ground state sublevels, is essentially correct, especially in the typical case in which dephasing rates are much smaller than spontaneous emission decay rates (see Eqs. (26)).

We then consider the numerical solution of the OBE and we compare it with the analytical treatment based on the AV approach presented above. The numerical calculations are performed in the range of parameters corresponding to EIT, i.e., $|\Omega_1|, |\Omega_2| \ll |\Omega_3|, |\Omega_4|$ and we stay near two-photon resonance for both the probe and the trigger field. In Figures 3–6 we compare the analytical solutions of equation (16) and equations (17) with the numerical solution of the complete set of Bloch equations given in the Appendix A. From these plots it is evident that our analytical treatment works satisfactorily well, except for a small interval of values of the detuning, corresponding to the maximum probe (or trigger) absorption. In such a case, the detunings match the Rabi frequencies of the two pumps, and the probe (or trigger) field is in resonance with a single atomic transition. The atoms are significantly pumped to the excited levels and the population assumption of equation (10) is not fulfilled. In fact, the discrepancy between the exact numerical solution of the OBE and the AV approach is strictly related to the atomic population out of level $|1\rangle$ which, in the case of Figure 3, is about 14% of the total population. Finally,

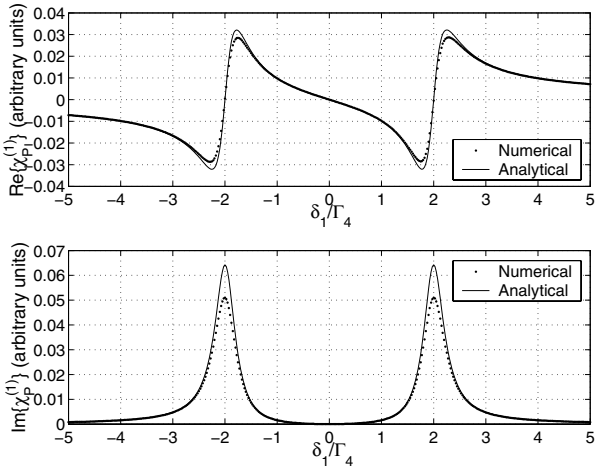

Fig. 3. Comparison of the numerical solution (dotted line) of the OBE with the analytical prediction of equation (16) (full line) for the real part (above) and imaginary part (below) of the linear probe susceptibility versus the normalized probe detuning δ_1/Γ_4. The parameter used are the following: $\Gamma_2^{AV} = \Gamma_2 = 36$ MHz, $\Gamma_4^{AV} = \Gamma_4 = 38$ MHz, $\delta_2 = \delta_3 = \delta_4 = 0$, $\forall i,j\ \gamma_{ij} = \Gamma_3^{AV} = \Gamma_5^{AV} = 10^{-4}\Gamma_4$, $\Omega_1 = 0.08\Gamma_4$, $\Omega_2 = 2\Gamma_4$, $\Omega_3 = 0.04\Gamma_4$, $\Omega_4 = \Gamma_4$.

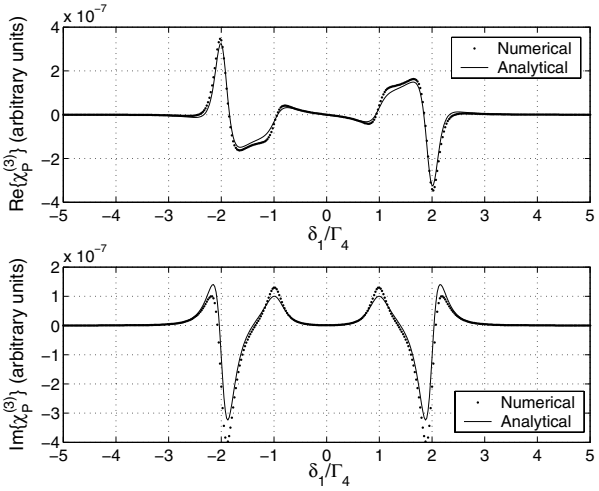

Fig. 4. Comparison of the numerical solution (dotted line) of the OBE with the analytical prediction of equation (17b) (full line) for the real part (above) and imaginary part (below) of the probe cross-Kerr susceptibility versus the normalized probe detuning δ_1/Γ_4. To reduce as much as possible the influence of the self-Kerr susceptibility we have considered a probe Rabi frequency Ω_1 much smaller than that of the trigger field. Parameters are: $\Gamma_2^{AV} = \Gamma_2 = 36$ MHz, $\Gamma_4^{AV} = \Gamma_4 = 38$ MHz, $\delta_2 = \delta_3 = \delta_4 = 0$, $\forall i,j\ \gamma_{ij} = \Gamma_3^{AV} = \Gamma_5^{AV} = 10^{-4}\Gamma_4$, $\Omega_1 = 0.004\Gamma_4$, $\Omega_2 = 2\Gamma_4$, $\Omega_3 = 0.04\Gamma_4$, $\Omega_4 = \Gamma_4$.

it should be mentioned that the success of the AV equation in describing the response of the atomic medium also significantly owes to the fact that in all cases of interest considered in this paper, the normalized equation is a very good approximation to the adiabatic condition (10). In other word, a very limited fraction of population ever appears in the excited states.

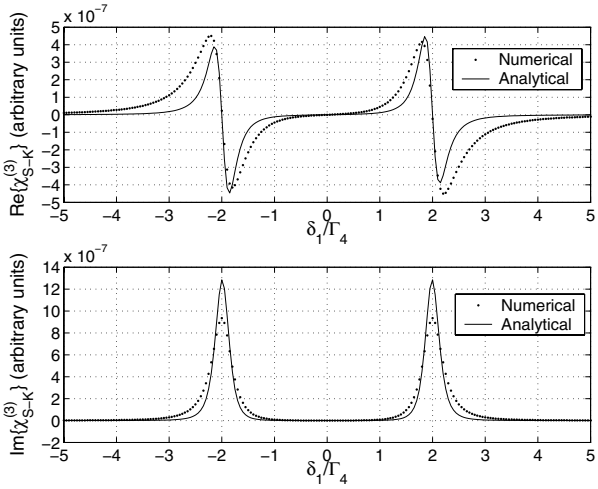

Fig. 5. Comparison of the numerical solution (dotted line) of the OBE with the analytical prediction of equation (17a) (full line) for the real part (above) and imaginary part (below) of the probe self-Kerr susceptibility versus the normalized probe detuning δ_1/Γ_4. To reduce as much as possible the influence of the cross-Kerr susceptibility we have considered a trigger Rabi frequency Ω_3 much smaller than that of the probe field. Parameters are: $\Gamma_2^{AV} = \Gamma_2 = 36$ MHz, $\Gamma_4^{AV} = \Gamma_4 = 38$ MHz, $\delta_2 = \delta_3 = \delta_4 = 0$, $\forall i,j\ \gamma_{ij} = \Gamma_3^{AV} = \Gamma_5^{AV} = 10^{-4}\Gamma_4$, $\Omega_1 = 0.5\Gamma_4$, $\Omega_2 = 2\Gamma_4$, $\Omega_3 = 0.005\Gamma_4$, $\Omega_4 = \Gamma_4$.

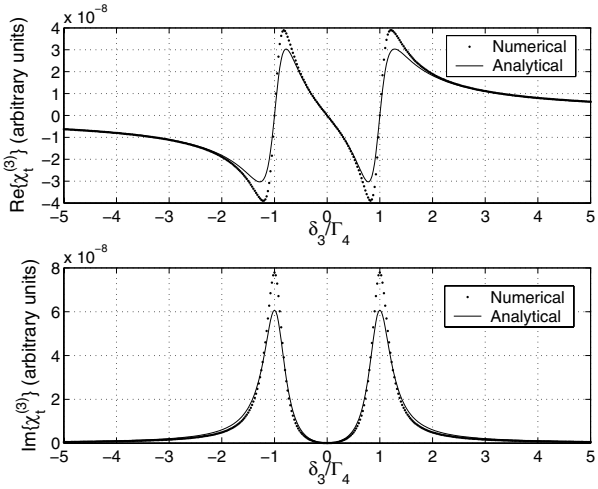

Fig. 6. Comparison of the numerical solution (dotted line) of the OBE with the analytical prediction of equation (17c) (full line) for the real part (above) and imaginary part (below) of the trigger cross-Kerr susceptibility as a function of the normalized trigger's detuning δ_3/Γ_4. Parameters are similar to those of Figure 3, $\Gamma_2^{AV} = \Gamma_2 = 36$ MHz, $\Gamma_4^{AV} = \Gamma_4 = 38$ MHz, $\delta_1 = \delta_2 = \delta_4 = 0$, $\forall i,j\ \gamma_{ij} = \Gamma_3^{AV} = \Gamma_5^{AV} = 10^{-4}\Gamma_4$, $\Omega_1 = 0.08\Gamma_4$, $\Omega_2 = 2\Gamma_4$, $\Omega_3 = 0.04\Gamma_4$, $\Omega_4 = \Gamma_4$.

Figures 3–6 refer to a situation with small dephasing rates ($\forall i,j,\ \gamma_{ij} = \Gamma_3^{AV} = \Gamma_5^{AV} = 10^{-4}\Gamma_4 \sim$ few kHz) which are typical for not too dense gases. For larger values of the dephasing rates (some tens of kHz), we have seen that the analytical prediction of the AV approach of the preceding subsection starts to depart from the exact solution of the OBE.

2.4 Group velocity matching

The propagation equation for the slowly varying electric field amplitudes $\varepsilon_i(z,t)$, $i = P,T$, defined as

$$\mathcal{E}_i(z,t) = \varepsilon_i(z,t)\exp\{ik_i z - i\omega_i t\} + c.c. \quad i = P,T,$$

is given by

$$\left(\frac{\partial}{\partial z} + \frac{1}{v_g^i}\frac{\partial}{\partial t}\right)\varepsilon_i(z,t) = i\frac{k_i}{2}\chi_i(z,t)\varepsilon_i(z,t), \quad i = P,T, \tag{27}$$

where v_g^i is the group velocity, generally defined as $v_g^i = c/(1+n_g^i)$, with c the speed of light in vacuum and

$$n_g^i = \frac{1}{2}\mathrm{Re}[\chi_i] + \frac{\omega_i}{2}\left(\frac{\partial \mathrm{Re}[\chi_i]}{\partial\omega}\right)_{\omega_i} \tag{28}$$

the group index, ω_i being the frequency of field i. The solution of equation (27) is

$$\varepsilon_i(z,t) = \varepsilon_i(0, t - \frac{z}{v_g^i})\exp\left\{i\frac{k_i}{2}\int_0^z dz'\chi_i(z',t)\right\}, \tag{29}$$

so that, using equations (15), the nonlinear cross-phase shift for the two fields of interest is given by

$$\phi_P^{ck} = \frac{\omega_1}{2c}\int_0^l dz \mathrm{Re}[\chi_P^{3,ck}]\,|\varepsilon_T(z,t)|^2\,, \tag{30a}$$

$$\phi_T^{ck} = \frac{\omega_3}{2c}\int_0^l dz \mathrm{Re}[\chi_T^{3,ck}]\,|\varepsilon_P(z,t)|^2\,, \tag{30b}$$

where l is the length of the atomic medium. These nonlinear cross-phase shifts are of fundamental importance also for quantum information processing applications. In fact, the CPS of equation (1) is determined only by these cross-Kerr contributions to the total phase shift, because the linear and self-Kerr contributions cancel out, as shown in references [14,15].

For Gaussian probe and trigger pulses of time durations τ_P and τ_T, and with peak Rabi frequencies Ω_P^{peak} and Ω_T^{peak} respectively, the nonlinear cross-phase shifts can be written as (see also Refs. [14,15])

$$\phi_P^{ck} = \frac{\omega_1 l}{4c}\frac{\sqrt{\pi}\hbar^2|\Omega_T^{peak}|^2}{|\mu_{34}|^2}\frac{\mathrm{erf}[\zeta_\mathrm{P}]}{\zeta_P}\mathrm{Re}[\chi_P^{3,ck}], \tag{31a}$$

$$\phi_T^{ck} = \frac{\omega_3 l}{4c}\frac{\sqrt{\pi}\hbar^2|\Omega_P^{peak}|^2}{|\mu_{12}|^2}\frac{\mathrm{erf}[\zeta_\mathrm{T}]}{\zeta_T}\mathrm{Re}[\chi_T^{3,ck}], \tag{31b}$$

where $\zeta_P = (1 - v_g^P/v_g^T)\sqrt{2}l/v_g^P\tau_T$ and ζ_T is obtained from ζ_P upon interchanging the indices $P \leftrightarrow T$. Large nonlinear cross-phase shifts take place for appreciably large values of the two cross-Kerr susceptibilities real parts, and especially when probe and trigger velocities become *equal*, i.e., when $\zeta_{P,T} \to 0$, in which case the $\mathrm{erf}[\zeta]/\zeta$ reaches the maximum value $2/\sqrt{\pi}$. In this limit the cross-phase phase shifts linearly increase with the length of the atomic medium l. This explains why achieving group velocity matching, $v_g^P = v_g^T$, is of fundamental importance. Moreover group velocities become small for large group indices and this condition can be achieved within the EIT transparency window, where $\mathrm{Re}[\chi]$ vanishes, and the group velocity is strongly reduced due to a large dispersion gradient $\partial\mathrm{Re}[\chi]/\partial\omega$.

Let us see how small and equal probe and trigger group velocities can be obtained. We consider the approximate analytical expressions for the susceptibilities of equations (15–17) derived above within the AV approach, and which we have seen to work very well in the EIT regime. Assuming to stay at the center of the transparency window for the probe ($\delta_{12} = 0$) where the dispersion gradient is maximum, and neglecting dephasing rates Γ_3^{AV} and Γ_5^{AV}, which are typically much smaller than all the other parameters, one gets

$$n_g^P \simeq \frac{N}{V}\frac{|\mu_{12}|^2\omega_1}{2\hbar\epsilon_0|\Omega_2|^2}(1 + |\Omega_3|^2\beta), \tag{32a}$$

$$n_g^T \simeq \frac{N}{V}\frac{|\mu_{34}|^2\omega_3}{2\hbar\epsilon_0|\Omega_2|^2}|\Omega_1|^2\beta, \tag{32b}$$

where [14]

$$\beta = \frac{\left(\delta_{14}^2 + |\Omega_4|^2\right)\left[\left(\delta_{13}\delta_{14} - |\Omega_4|^2\right)^2 - \delta_{14}^2\left(\Gamma_4^{AV}/2\right)^2\right]}{\left[\left(\delta_{13}\delta_{14} - |\Omega_4|^2\right)^2 + \delta_{14}^2\left(\Gamma_4^{AV}/2\right)^2\right]^2}. \tag{33}$$

In the EIT situation we are considering it is $n_g^P, n_g^T \gg 1$, so that, using equations (32),

$$v_g^P \simeq \frac{c}{n_g^P} \simeq \frac{2\hbar\epsilon_0 c|\Omega_2|^2}{(N/V)|\mu_{12}|^2\omega_1(1 + |\Omega_3|^2\beta)}, \tag{34a}$$

$$v_g^T \simeq \frac{c}{n_g^T} \simeq \frac{2\hbar\epsilon_0 c|\Omega_2|^2}{(N/V)|\mu_{34}|^2\omega_3|\Omega_1|^2\beta}. \tag{34b}$$

As expected, the asymmetric M-scheme does not yield equal slow down of both trigger and probe pulse automatically as, for example, the scheme of Petrosyan and Kurizki [16] does. In fact, the two expressions of the group velocities are generally different. Nonetheless, equations (34) show that group velocity matching is always achievable by properly adjusting the parameter β, which means adjusting the tuner intensity $|\Omega_4|^2$ and the composite detuning δ_{14}. This shows that the present asymmetric M-scheme can be seen as a modified version of the N-scheme of reference [5], in which the tuner pump field is added just in order to "tune" the group velocity of the trigger pulse so to make it equal to that of the probe. The possibility to achieve group velocity matching is shown in Figure 7, where both the numerical result derived from the OBE and the approximate analytical expressions of equations (34) are plotted versus the trigger detuning δ_3. Two different values of δ_3 exist for which $v_g^P = v_g^T \simeq 1000$ m/s (see Fig. 7). Parameter values here correspond to typical values for a cell of ^{87}Rb atoms, i.e., $\Gamma_2^{AV} = \Gamma_2 \simeq 36$ MHz, $\Gamma_4^{AV} = \Gamma_4 \simeq 38$ MHz, $N/V \simeq 3\times10^{13}$ cm^{-3}, $\delta_1 = \delta_2 = 0$, $\delta_4 \simeq \delta_3 \simeq 20\Gamma_4$, $\Omega_1 = 0.08\Gamma_4$, $\Omega_2 = 2\Gamma_4$, $\Omega_3 = 0.04\Gamma_4$,

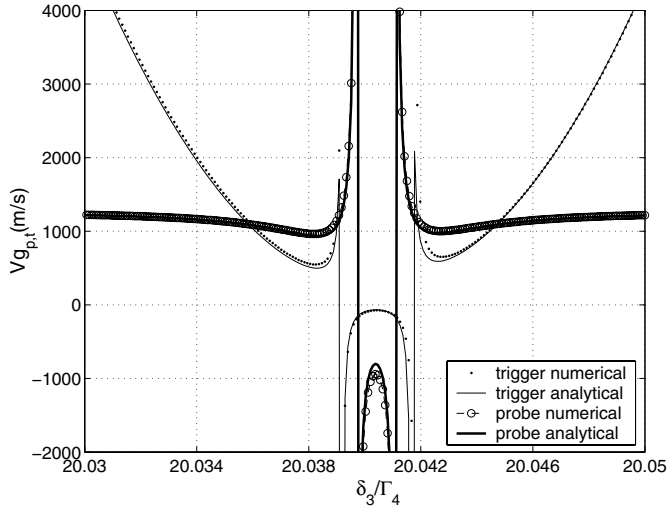

Fig. 7. Group velocity of the probe and trigger pulses versus the normalized trigger detuning δ_3/Γ_4. Full lines denote the analytical predictions of equations (34) (the thick line refers to the probe and the thin line to the trigger). Circles and dots refer to the numerical solution of the OBE for the probe and trigger group velocity, respectively. This figure shows how it is possible to obtain group velocity matching in the asymmetric M-scheme: two different values of δ_3 exist for which $v_g^P = v_g^T \simeq 1000$ m/s. The parameters are those of the D_1 and D_2 line in the ^{87}Rb spectrum: $\Gamma_2^{AV} = \Gamma_2 \simeq 36$ MHz, $\Gamma_4^{AV} = \Gamma_4 \simeq 38$ MHz, $\delta_1 = \delta_2 = 0$, $\delta_4 \simeq \delta_3 \simeq 20\Gamma_4$, $\Omega_1 = 0.08\Gamma_4$, $\Omega_2 = 2\Gamma_4$, $\Omega_3 = 0.04\Gamma_4$, $\Omega_4 = \Gamma_4$, $\forall i,j$, $\gamma_{ij} = \Gamma_3^{AV} = \Gamma_5^{AV} = 10^{-4}\Gamma_4$, $N/V = 3.0 \times 10^{13}$ cm^{-3}.

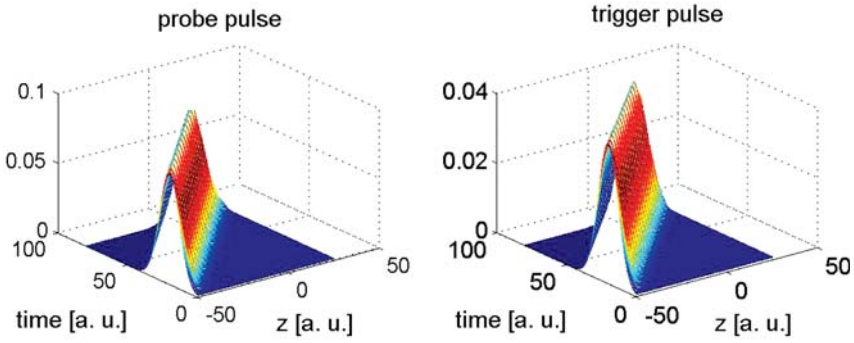

Fig. 8. (Color online) Propagation of probe and trigger pulses through the asymmetric M medium. Pulses are taken to be Gaussian at time $t = 0$ and are sufficiently long ($\tau_i > 1/\Delta\omega_{tr}^i$), $i = P, T$. Units are arbitrary, with $c = 1$.

$\Omega_4 = \Gamma_4$, $\forall i,j$, $\gamma_{ij} = \Gamma_3^{AV} = \Gamma_5^{AV} = 10^{-4}\Gamma_4$. Moreover Figure 7 clearly shows that the simple expressions of equations (34) well reproduce the exact numerical solution of the OBE.

2.5 Pulse propagation

In previous section, we have addressed the problem of group velocity matching between probe and trigger fields in the asymmetric M-scheme. It should be emphasized that the analysis and the results presented there are strictly valid for the continuous-wave (cw) fields. We would now address that same problem but with the pulsed probe and trigger fields in mind. At the first look, equations (34) appear to suggest that the group velocity matching would not be possible in the pulsed regime. As the group velocity of the trigger pulse is inversely proportional to the square of the probe pulse, trigger suffers anomalous dispersion, i.e. in the presence of a pulsed probe, the trigger pulse will get distorted, splitting into several components, each having a different group velocity.

It will be shown in this Section that the above conclusion is an artifact of approximations made to obtain a closed and compact expression for group velocities. In particular, the pulse propagation in this approximation is described by equations (27), with group velocities v_g^i given by equations (34) and nonlinear susceptibilities χ_i being those of equations (17). This is equivalent to the adiabatic elimination of the atomic degrees of freedom. Such adiabatic elimination, strictly speaking, is not valid in the parameter regime explored in this paper: strong nonlinear interaction between probe and trigger pulses suggests that the contribution of the atomic medium is far from being adiabatic. Also, it should be noted that the dephasing processes have been neglected in the derivation of v_g^i. For the adiabatic case, the above conclusion is correct: the trigger pulse suffers anomalous dispersion and its group velocity becomes singular towards the edges of a probe pulse. However, pulse propagation through the asymmetric M-system do not follow such a simple approximate evolution. Full propagation problem must then be solved which includes adding the time-dependent equations for the pulses

$$\left(\frac{\partial}{\partial z} + \frac{1}{c}\frac{\partial}{\partial t}\right)\varepsilon_i(z,t) = i\frac{k_i}{2}\frac{N\mu_i}{V\epsilon_0}\sigma_i(z,t), \quad i = P,T, \quad (35)$$

to the OBEs [Eqs. (A.1, A.2)], and numerically solving the resulting system of equations. In the above equation, it is understood that $\sigma_P = \sigma_{12}$ and $\sigma_T = \sigma_{34}$ in the notation of equations (A.2).

Results are shown in Figures 8 and 9 for the same set of parameters that yields group velocities matching in Figure 7. Vertical axes have been scaled appropriately to obtain Rabi frequencies Ω_i. Two operating regimes could be identified, long-pulse regime and short-pulse regime,

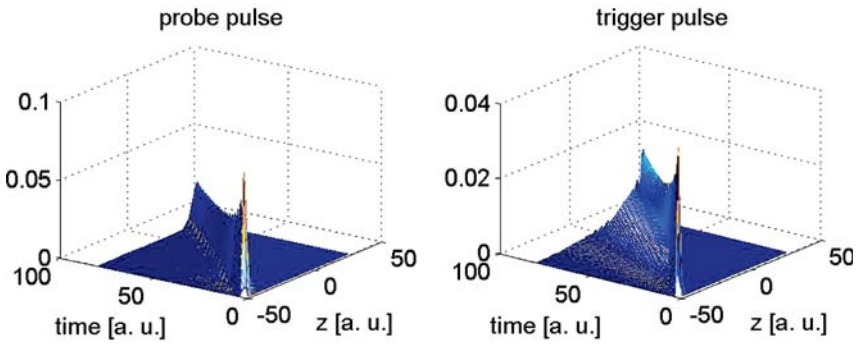

Fig. 9. (Color online) Propagation of probe and trigger pulses through the asymmetric M medium. Pulses are taken to be Gaussian at time $t = 0$ and short ($\tau_i < 1/\Delta\omega_{tr}^i$), $i = P, T$. Units are arbitrary, with $c = 1$.

where 'long' and 'short' denotes the pulses' length in time. This length is compared to the inverse width of the transparency window. Long pulses fit well into the transparency window, while short pulses do not. Figure 8 shows the results of our simulation for the initially identical long Gaussian pulses. It is clear that the pulses propagate undistorted with the equal group velocities. Tiny amplitude decay is present due to the small imaginary part of the nonlinear susceptibility.

Short pulses (Fig. 9) however, show distortion. Probe pulse distortion comes from the absorption, as the pulse spreads outside of the transparency window. Trigger pulse shows the same absorption effect, but moreover it also splits into several components which then continue to propagate with a different group velocities each. Note that the singularity present in the adiabatic approach is not present here. This is due to the fact that the dephasing, neglected in the adiabatic treatment, effectively *regularizes* the equations, removing the singularity.

It is also noted that in the long-pulse regime, both of the pulses propagate virtually undistorted, with a group velocity uniform across each of the pulses. Our simulations suggest that the approximate equations (34) are valid, as long as the Rabi frequencies there are considered to be taken at the *peak* of the pulse, i.e. $\Omega_i \to \Omega_i^{peak}$.

3 The symmetric M–scheme

In this section we analyze the symmetric M–scheme, schematically shown in Figure 10. The initial conditions and the configuration of the fields are slightly different from those of the asymmetric case of Section 2. The same five levels could be used, but all the atoms are now initially prepared in level $|3\rangle$ (see Fig. 10). Moreover, the role of the probe and of the coupler fields are exchanged, i.e., now the probe field (still with Rabi frequency Ω_1 and central frequency ω_1) couples levels $|2\rangle$ and $|3\rangle$, while the coupler (still with Rabi frequency Ω_2 and central frequency ω_2) induces transitions between levels $|1\rangle$ and $|2\rangle$. The role of trigger and tuner fields remains unchanged. In such a way, the scheme becomes symmetric for probe and trigger, and the two fields experience *exactly* the same dynamics whenever the corresponding parameters are made equal, i.e., when the Rabi frequencies are correspondingly equal ($\Omega_1 = \Omega_3$, $\Omega_2 = \Omega_4$), as well as the detunings, ($\delta_1 = \delta_3$, $\delta_2 = \delta_4$), which are now defined similarly to those of the asymmetric M scheme (see Eqs. (3)) except for probe-coupler exchange, i.e.,

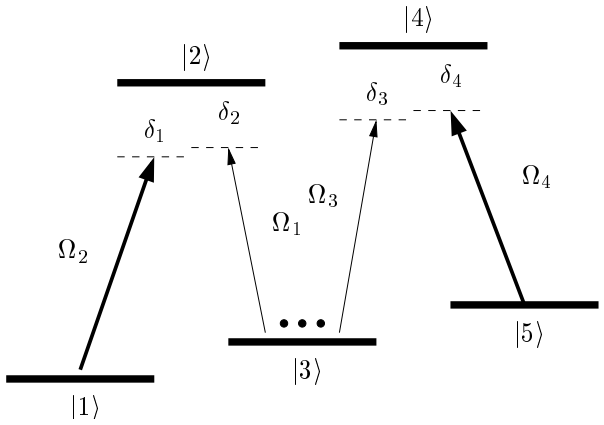

Fig. 10. Symmetric M scheme. The probe and the trigger fields, with Rabi frequencies Ω_1 and Ω_3 respectively, together with the stronger pump fields, the coupler and the tuner (with Rabi frequencies Ω_2 and Ω_4, respectively) drive the corresponding transitions. All the atoms are assumed to be in state $|3\rangle$ and the detunings are defined in equations (36).

$$E_2 - E_1 = \hbar\omega_2 + \hbar\delta_2, \tag{36a}$$
$$E_2 - E_3 = \hbar\omega_1 + \hbar\delta_1, \tag{36b}$$
$$E_4 - E_3 = \hbar\omega_3 + \hbar\delta_3, \tag{36c}$$
$$E_4 - E_5 = \hbar\omega_4 + \hbar\delta_4. \tag{36d}$$

In this way, the scheme can be seen again as formed by two adjacent Λ, one for the probe and one for the trigger, now however symmetrically placed with respect to state $|3\rangle$. As we have done for the asymmetric M scheme, we assume to stay close to the two-photon resonance conditions, $\delta_1 \simeq \delta_2$ and $\delta_3 \simeq \delta_4$, and moreover that $|\Omega_1| \ll |\Omega_2|$, and $|\Omega_3| \ll |\Omega_4|$, so that both probe and trigger will experience EIT. As we have seen above, a large XPM is obtained when the group velocities are equal [10,14–16,18,22], and the advantage of the present symmetric M–scheme is that group velocity matching is automatically achieved once that the scheme is exactly symmetric between probe and trigger.

The Hamiltonian of the system is

$$H_S = \sum_i^5 E_i|i\rangle\langle i| + \hbar\left(\Omega_1 e^{-i\omega_1 t}|2\rangle\langle 3| + \Omega_2 e^{-i\omega_2 t}|2\rangle\langle 1| + \Omega_3 e^{-i\omega_3 t}|4\rangle\langle 3| + \Omega_4 e^{-i\omega_4 t}|4\rangle\langle 5| + h.c.\right). \quad (37)$$

Moving to the interaction picture with respect to the following free Hamiltonian

$$H_0' = E_3|3\rangle\langle 3| + (E_2 - \hbar\delta_1)|2\rangle\langle 2| + (E_1 - \hbar\delta_{12})|1\rangle\langle 1| + (E_4 - \hbar\delta_3)|4\rangle\langle 4| + (E_5 - \hbar\delta_{34})|5\rangle\langle 5|, \quad (38)$$

where

$$\delta_{12} = \delta_1 - \delta_2, \quad (39a)$$
$$\delta_{34} = \delta_3 - \delta_4, \quad (39b)$$

we get the following effective Hamiltonian

$$H_{eff}^S = \hbar\delta_1|2\rangle\langle 2| + \hbar\delta_{12}|1\rangle\langle 1| + \hbar\delta_3|4\rangle\langle 4| + \hbar\delta_{34}|5\rangle\langle 5| + \hbar\Omega_1|2\rangle\langle 3| + \hbar\Omega_2|2\rangle\langle 1| + \hbar\Omega_3|4\rangle\langle 3| + \hbar\Omega_4|4\rangle\langle 5| + \hbar\Omega_1^\star|3\rangle\langle 2| + \hbar\Omega_2^\star|1\rangle\langle 2| + \hbar\Omega_3^\star|3\rangle\langle 4| + \hbar\Omega_4^\star|5\rangle\langle 4|. \quad (40)$$

3.1 Amplitude variables approach

We first study the system dynamics by means of the AV approach, in which the state of the atom is described by the wave-function of equation (8), whose time evolution is determined by the Hamiltonian of equation (40), supplemented with phenomenological decay rates Γ_i^{AV} for each atomic level $|i\rangle$. The corresponding evolution equations for the amplitudes $b_i(t)$ are

$$\dot{b}_1(t) = -\imath d_1 b_1(t) - \imath\Omega_2^\star b_2(t), \quad (41a)$$
$$\dot{b}_2(t) = -\imath d_2 b_2(t) - \imath\Omega_2 b_1(t) - \imath\Omega_1 b_3(t), \quad (41b)$$
$$\dot{b}_3(t) = -\imath d_3 b_3 - \imath\Omega_1^\star b_2(t) - \imath\Omega_3^\star b_4(t), \quad (41c)$$
$$\dot{b}_4(t) = -\imath d_4 b_4(t) - \imath\Omega_3 b_3(t) - \imath\Omega_4 b_5(t), \quad (41d)$$
$$\dot{b}_5(t) = -\imath d_5 b_5(t) - \imath\Omega_4^\star b_4(t), \quad (41e)$$

where, similarly to what we have done for the asymmetric case, we have defined

$$d_1 = \delta_{12} - \imath\Gamma_1^{AV}/2, \quad (42a)$$
$$d_2 = \delta_1 - \imath\Gamma_2^{AV}/2, \quad (42b)$$
$$d_3 = -\imath\Gamma_3^{AV}/2, \quad (42c)$$
$$d_4 = \delta_3 - \imath\Gamma_4^{AV}/2, \quad (42d)$$
$$d_5 = \delta_{34} - \imath\Gamma_5^{AV}/2. \quad (42e)$$

Since we choose again $|\Omega_1/\Omega_2| \ll 1$ and $|\Omega_3/\Omega_4| \ll 1$, it is reasonable to assume that the atomic population remains in the initial state $|3\rangle$ to a good approximation

$$b_3^{ss} \sim 1. \quad (43)$$

The set of equations (41) is then solved in the steady-state. In order to get a consistent expression for the nonlinear susceptibilities one has to consider higher order contributions to equation (43), which is obtained by imposing the normalization of the atomic wave-function of equation (8) at second order in $|\Omega_1/\Omega_2|$ and $|\Omega_3/\Omega_4|$. One gets the following expression for the steady state amplitudes

$$b_3^{ss} = 1 - \frac{|\Omega_1|^2\left[|d_1|^2 + |\Omega_2|^2\right]}{2\left|d_1 d_2 - |\Omega_2|^2\right|^2} - \frac{|\Omega_3|^2\left[|d_5|^2 + |\Omega_4|^2\right]}{2\left|d_4 d_5 - |\Omega_4|^2\right|^2}, \quad (44a)$$

$$b_2^{ss} = -\frac{\Omega_1 d_1}{d_1 d_2 - |\Omega_2|^2} b_3^{ss}, \quad (44b)$$

$$b_4^{ss} = -\frac{\Omega_3 d_5}{d_5 d_4 - |\Omega_4|^2} b_3^{ss}, \quad (44c)$$

$$b_1^{ss} = \frac{\Omega_1\Omega_2^\star}{d_1 d_2 - |\Omega_2|^2} b_3^{ss}, \quad (44d)$$

$$b_5^{ss} = \frac{\Omega_3\Omega_4^\star}{d_5 d_4 - |\Omega_4|^2} b_3^{ss}. \quad (44e)$$

These results can be used to determine the probe and trigger susceptibilities, which are now defined as (see Eqs. (14))

$$\chi_P = \frac{N\mu_{32}}{V\varepsilon_0\mathcal{E}_1} b_2^{ss} b_3^{ss,\star} = -\frac{N|\mu_{32}|^2}{V\hbar\varepsilon_0\Omega_1} b_2^{ss} b_3^{ss,\star}, \quad (45a)$$

$$\chi_T = \frac{N\mu_{34}}{V\varepsilon_0\mathcal{E}_3} b_4^{ss} b_3^{ss,\star} = -\frac{N|\mu_{34}|^2}{V\hbar\varepsilon_0\Omega_3} b_4^{ss} b_3^{ss,\star}. \quad (45b)$$

Inserting equations (44) into equations (45) and expanding in series at the lowest orders in the probe and trigger electric fields, $\mathcal{E}_1$ and $\mathcal{E}_3$ respectively, one gets

$$\chi_P \simeq \chi_P^{(1)} + \chi_P^{(3,sk)}|\mathcal{E}_1|^2 + \chi_P^{(3,ck)}|\mathcal{E}_3|^2, \quad (46a)$$

$$\chi_T \simeq \chi_T^{(1)} + \chi_T^{(3,sk)}|\mathcal{E}_3|^2 + \chi_T^{(3,ck)}|\mathcal{E}_1|^2, \quad (46b)$$

where we have again distinguished the third-order self-Kerr susceptibilities $\chi_{P,T}^{(3,sk)}$ from the third-order cross-Kerr susceptibilities $\chi_{P,T}^{(3,ck)}$. Using equations (44) and the definitions of equations (42), we get the following expressions for the linear susceptibilities,

$$\chi_P^{(1)} = \frac{N|\mu_{32}|^2}{V\hbar\varepsilon_0} \frac{\delta_{12} - i\Gamma_1^{AV}/2}{\left(\delta_1 - i\Gamma_2^{AV}/2\right)\left(\delta_{12} - i\Gamma_1^{AV}/2\right) - |\Omega_2|^2} \quad (47a)$$

$$\chi_T^{(1)} = \frac{N|\mu_{34}|^2}{V\hbar\varepsilon_0} \frac{\delta_{34} - i\Gamma_5^{AV}/2}{\left(\delta_3 - i\Gamma_4^{AV}/2\right)\left(\delta_{34} - i\Gamma_5^{AV}/2\right) - |\Omega_4|^2} \quad (47b)$$

$$\chi_P^{(3,sk)} = \frac{N|\mu_{32}|^4}{V\hbar^3\varepsilon_0} \frac{-\left(\delta_{12} - i\Gamma_1^{AV}/2\right)\left[\left|\delta_{12} - i\Gamma_1^{AV}/2\right|^2 + |\Omega_2|^2\right]}{\left[\left(\delta_1 - i\Gamma_2^{AV}/2\right)\left(\delta_{12} - i\Gamma_1^{AV}/2\right) - |\Omega_2|^2\right]\left|\left(\delta_1 - i\Gamma_2^{AV}/2\right)\left(\delta_{12} - i\Gamma_1^{AV}/2\right) - |\Omega_2|^2\right|^2}, \tag{48a}$$

$$\chi_T^{(3,sk)} = \frac{N|\mu_{34}|^4}{V\hbar^3\varepsilon_0} \frac{-\left(\delta_{34} - i\Gamma_5^{AV}/2\right)\left[\left|\delta_{34} - i\Gamma_5^{AV}/2\right|^2 + |\Omega_4|^2\right]}{\left[\left(\delta_3 - i\Gamma_4^{AV}/2\right)\left(\delta_{34} - i\Gamma_5^{AV}/2\right) - |\Omega_4|^2\right]\left|\left(\delta_3 - i\Gamma_4^{AV}/2\right)\left(\delta_{34} - i\Gamma_5^{AV}/2\right) - |\Omega_4|^2\right|^2}, \tag{48b}$$

$$\chi_P^{(3,ck)} = \frac{N|\mu_{32}|^2|\mu_{34}|^2}{V\hbar^3\varepsilon_0} \frac{-\left(\delta_{12} - i\Gamma_1^{AV}/2\right)\left[\left|\delta_{34} - i\Gamma_5^{AV}/2\right|^2 + |\Omega_4|^2\right]}{\left[\left(\delta_1 - i\Gamma_2^{AV}/2\right)\left(\delta_{12} - i\Gamma_1^{AV}/2\right) - |\Omega_2|^2\right]\left|\left(\delta_3 - i\Gamma_4^{AV}/2\right)\left(\delta_{34} - i\Gamma_5^{AV}/2\right) - |\Omega_4|^2\right|^2}, \tag{48c}$$

$$\chi_T^{(3,ck)} = \frac{N|\mu_{32}|^2|\mu_{34}|^2}{V\hbar^3\varepsilon_0} \frac{-\left(\delta_{34} - i\Gamma_5^{AV}/2\right)\left[\left|\delta_{12} - i\Gamma_1^{AV}/2\right|^2 + |\Omega_2|^2\right]}{\left[\left(\delta_3 - i\Gamma_4^{AV}/2\right)\left(\delta_{34} - i\Gamma_5^{AV}/2\right) - |\Omega_4|^2\right]\left|\left(\delta_1 - i\Gamma_2^{AV}/2\right)\left(\delta_{12} - i\Gamma_1^{AV}/2\right) - |\Omega_2|^2\right|^2}. \tag{48d}$$

and the following ones for the nonlinear susceptibilities,

see equations (48) above.

First of all we note that the expressions of the probe and trigger susceptibilities above are completely symmetric. This means that probe and trigger experience the same linear and Kerr susceptibilities, as soon as the corresponding parameters correspond, i.e., $\mu_{32} = \mu_{34}$, $\Omega_1 = \Omega_3$, $\Omega_2 = \Omega_4$, $\delta_1 = \delta_3$, $\delta_2 = \delta_4$, $\Gamma_1^{AV} = \Gamma_5^{AV}$, $\Gamma_2^{AV} = \Gamma_4^{AV}$. Moreover, the probe linear susceptibility of equation (47a) and the self-Kerr susceptibility of equation (48a) coincide with the corresponding ones of the asymmetric case, equations (16) and (17a) respectively, because the phenomenological decay rate Γ_1^{AV} here plays just the same role of the phenomenological decay rate Γ_3^{AV} of the asymmetric scheme. This is not surprising, since the probe response in the absence of the trigger field is the same in the two M scheme studied here. Finally the cross-Kerr susceptibilities of the two schemes are generally different, both for the probe and the trigger, even though they possess a similar structure. The main relevant difference between the two cross-Kerr susceptibilities is in the dependence of their real parts upon the detunings. In fact, in the asymmetric case both real parts are proportional to the composite detuning $\delta_{14} = \delta_{12} + \delta_{34}$ (see Eqs. (6) and (39)), so that one has a nonzero XPM as soon as one of the two Λ subsystem is shifted from the two-photon resonance condition. In the symmetric case instead, $\mathrm{Re}\{\chi_P^{(3,ck)}\}$ is proportional to δ_{12} and $\mathrm{Re}\{\chi_T^{(3,ck)}\}$ is proportional to δ_{34}, and the two-photon resonance condition has to be violated by *both* Λ subsystems if each field has to experience a nonzero XPM.

3.2 Comparison with the optical Bloch equations

We now study the dynamics of the symmetric M scheme of Figure 10 by means of the OBE, which allow to describe spontaneous emission and dephasing more rigorously. Due to the similarity of the symmetric and asymmetric M schemes, we consider the same spontaneous emission and dephasing processes described in Section 2.3. As a consequence, the master equation for the atomic density operator ρ is again given by equation (19), with the only difference that the Hamiltonian H_{eff}^{AS} is replaced by the corresponding Hamiltonian H_{eff}^{S} of the symmetric scheme, given by equation (40). The corresponding system of OBE's for the mean values $\sigma_{ij}(t) \equiv \langle\hat{\sigma}_{ij}(t)\rangle \equiv \rho_{ji}(t)$ is displayed in Appendix B as equations (B.1) and (B.2), where we have used the definitions of equations (20–22). Comparison proceeds following the same logic as used in Section 2.

Also in this symmetric case, the OBE are less suited for an approximate analytical treatment with respect to the AV equations of the preceding subsection. In fact, if we consider the conditions $|\Omega_1/\Omega_2| \ll 1$ and $|\Omega_3/\Omega_4| \ll 1$ and, consistently with equation (43), we assume that

$$\sigma_{33} \approx 1, \tag{49a}$$

$$\sigma_{jj} \approx 0, \quad j = 1, 2, 4, 5, \tag{49b}$$

at the steady state, it is possible to see that by inserting equations (23) into equations (B.2) for the coherences, one gets a satisfactory expression for the probe linear susceptibility only. To be more specific, only the approximate linear susceptibility fits well with the numerical solution of the OBE. It is not easy to derive analytical expressions from equations (B.1) and (B.2) for the nonlinear susceptibilities which would be as simple as those of equations (48) and which would reproduce in the same way the exact numerical solution of the OBE within the EIT regime. Again, one could exactly solve analytically the OBE, but the resulting expressions are very cumbersome and not physically transparent as those of equations (48). For this reason we will analytically derive from the OBE the probe linear susceptibility only, and we will then use the OBE only for the numerical determination of the atomic steady state. In addition, deriving this result will enable us to draw a formal analogy between the AV and OBE treatments (see Eqs. (52) below).

The probe and trigger susceptibilities are now defined as

$$\chi_P = \frac{N\mu_{32}}{V\varepsilon_0\mathcal{E}_1}\sigma_{32} = -\frac{N|\mu_{32}|^2}{V\hbar\varepsilon_0\Omega_1}\sigma_{32}, \tag{50a}$$

$$\chi_T = \frac{N\mu_{34}}{V\varepsilon_0\mathcal{E}_3}\sigma_{34} = -\frac{N|\mu_{34}|^2}{V\hbar\varepsilon_0\Omega_3}\sigma_{34}. \tag{50b}$$

Using equations (49) and performing a series expansion at the lowest order in the probe and trigger fields, we arrive at the following expressions for the probe and trigger linear susceptibilities

$$\chi_P^{(1)} = \frac{N|\mu_{32}|^2}{V\hbar\varepsilon_0} \frac{\delta_{12} - i\gamma_{13}/2}{[\delta_{12} - i\gamma_{13}/2]\,[\delta_1 - i\,(\Gamma_2 + \gamma_{12})\,/2] - |\Omega_2|^2}, \tag{51a}$$

$$\chi_T^{(1)} = \frac{N|\mu_{34}|^2}{V\hbar\varepsilon_0} \frac{\delta_{34} - i\gamma_{53}/2}{[\delta_{34} - i\gamma_{53}/2]\,[\delta_3 - i\,(\Gamma_4 + \gamma_{54})\,/2] - |\Omega_4|^2}. \tag{51b}$$

Due to the symmetry of the scheme, the probe linear susceptibility coincides with that of the trigger of equation (51b) when the corresponding parameters coincide, i.e., $\mu_{32} = \mu_{34}$, $\delta_1 = \delta_3$, $\delta_2 = \delta_4$, $\Omega_2 = \Omega_4$, $\Gamma_2 = \Gamma_4$, $\gamma_{54} = \gamma_{12}$ and $\gamma_{53} = \gamma_{13}$. By comparing equations (51) with equations (47), one can also see that the AV and OBE predictions for the linear susceptibilities again coincide provided that the phenomenological decay rates Γ_i^{AV} are appropriately interpreted, i.e.,

$$\Gamma_2^{AV} \leftrightarrow \Gamma_2 + \gamma_{12}, \tag{52a}$$

$$\Gamma_1^{AV} \leftrightarrow \gamma_{13}, \tag{52b}$$

$$\Gamma_4^{AV} \leftrightarrow \Gamma_4 + \gamma_{54}, \tag{52c}$$

$$\Gamma_5^{AV} \leftrightarrow \gamma_{53}. \tag{52d}$$

This shows again that the intuitive interpretation of the phenomenological decay rates Γ_i^{AV} as spontaneous emission total decay rates for the excited states, and as dephasing rates in the case of ground state sublevels, is essentially correct.

We then consider the numerical solution of the OBE and we compare it with the analytical treatment based on the AV approach. In Figures 11–13 we compare the analytical solutions of equations (47) and (48) with the numerical solution of the complete set of Bloch equations given in Appendix B. Figure 11 shows the linear susceptibilities and refers to a perfectly symmetric situation between probe and trigger. As a consequence, the probe and trigger linear susceptibilities as a function of the respective detunings δ_1 and δ_3 are two indistinguishable curves. In such a case, group velocity matching is automatically guaranteed whenever $\mu_{32} = \mu_{34}$. Figure 12 shows the cross-Kerr susceptibilities again in a perfectly symmetric situation between probe and trigger so that their plots as a function of the respective detunings δ_1 and δ_3 exactly coincide. Finally Figure 13 shows the self-Kerr susceptibilities again in a perfectly symmetric situation between probe and trigger. As a consequence their plots versus the respective detunings δ_1 and δ_3 exactly coincide.

3.3 Group velocity matching

As we have seen in Section 2.4, the condition of group velocity matching is of fundamental importance for achieving a large cross-phase modulation between probe and trigger fields. It is evident from the inherent symmetry of

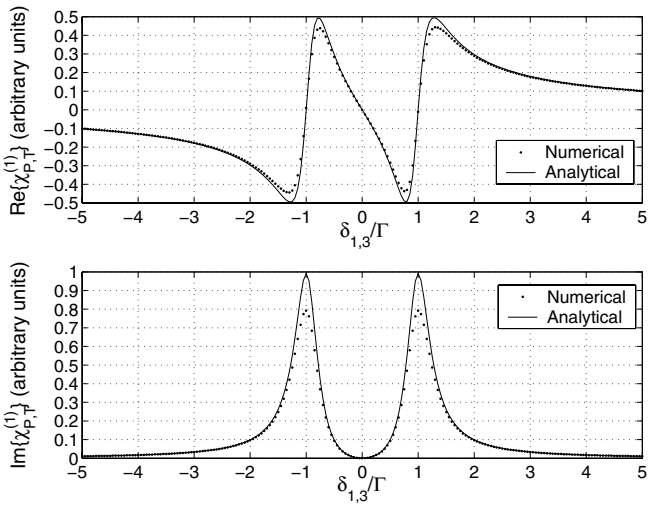

Fig. 11. Comparison of the numerical solution (dotted line) of the OBE with the analytical prediction of equations (47) (full line) for the real part (above) and imaginary part (below) of both probe and trigger linear susceptibilities versus their respective normalized probe detunings δ_1/Γ and δ_3/Γ. Probe and trigger susceptibilities exactly overlap because we consider the perfectly symmetric situation $\Gamma_2^{AV} = \Gamma_2 = \Gamma_4^{AV} = \Gamma_4 = \Gamma = 2\pi\times 6$ MHz, $\Omega_1 = \Omega_3 = 0.08\Gamma$, $\Omega_2 = \Omega_4 = \Gamma$, $\delta_2 = \delta_4 = 0$, $\forall i,j\ \gamma_{ij} = \Gamma_1^{AV} = \Gamma_5^{AV} = 10^{-4}\Gamma$, $\mu_{32} = \mu_{34}$, which guarantees perfect group velocity matching.

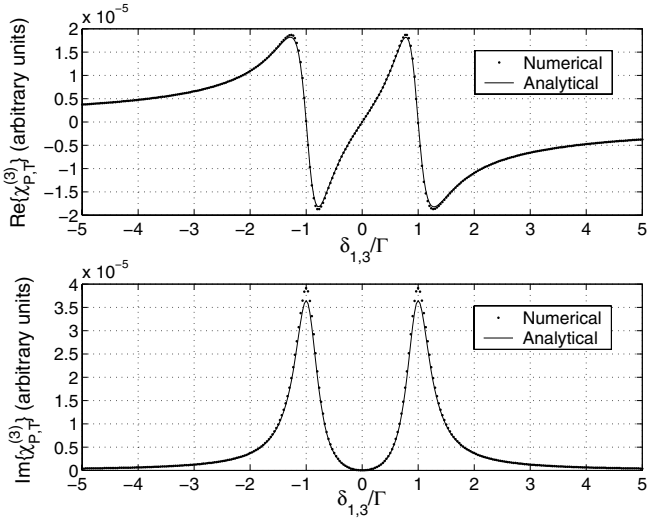

Fig. 12. Comparison of the numerical solution (dotted line) of the OBE with the analytical prediction of equations (48c, 48d) (full line) for the real part (above) and imaginary part (below) of both probe and trigger cross-Kerr susceptibilities versus their respective normalized probe detunings δ_1/Γ and δ_3/Γ. Probe and trigger susceptibilities exactly overlap because we consider a perfectly symmetric situation: $\Gamma_2^{AV} = \Gamma_2 = \Gamma_4^{AV} = \Gamma_4 = \Gamma = 2\pi \times 6$ MHz, $\Omega_2 = \Omega_4 = \Gamma$, $\delta_2 = \delta_4 = 0$, $\forall i,j\ \gamma_{ij} = \Gamma_1^{AV} = \Gamma_5^{AV} = 10^{-4}\Gamma$; moreover we have chosen $\Omega_1 = 0.002\Gamma$, $\Omega_3 = 0.08\Gamma$ in the case of the $\chi_P^{(3,ck)}$ plot, and vice versa $\Omega_3 = 0.002\Gamma$, $\Omega_1 = 0.08\Gamma$ in the case of the $\chi_T^{(3,ck)}$ plot, in order to reduce as much as possible the influence of the self-Kerr susceptibilities.

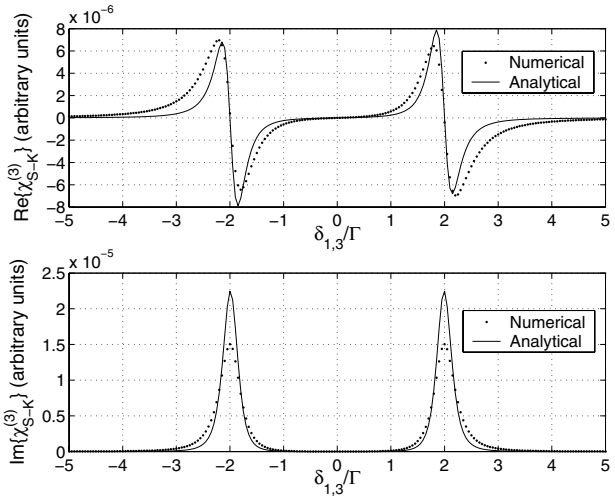

Fig. 13. Comparison of the numerical solution (dotted line) of the OBE with the analytical prediction of equations (48a, 48b) (full line) for the real part (above) and imaginary part (below) of both probe and trigger self-Kerr susceptibilities versus their respective normalized probe detunings δ_1/Γ and δ_3/Γ. Probe and trigger susceptibilities exactly overlap because we consider a perfectly symmetric situation: $\Gamma_2^{AV} = \Gamma_2 = \Gamma_4^{AV} = \Gamma_4 = \Gamma = 2\pi \times 6$ MHz, $\Omega_2 = \Omega_4 = 2\Gamma$, $\delta_2 = \delta_4 = 0$, $\forall i,j$ $\gamma_{ij} = \Gamma_1^{AV} = \Gamma_5^{AV} = 10^{-4}\Gamma$; moreover we have chosen $\Omega_1 = 0.4\Gamma$, $\Omega_3 = 0.004\Gamma$ in the case of the $\chi_P^{(3,sk)}$ plot, and vice versa $\Omega_3 = 0.4\Gamma$, $\Omega_1 = 0.004\Gamma$ in the case of the $\chi_T^{(3,sk)}$ plot, in order to reduce as much as possible the influence of the cross-Kerr susceptibilities.

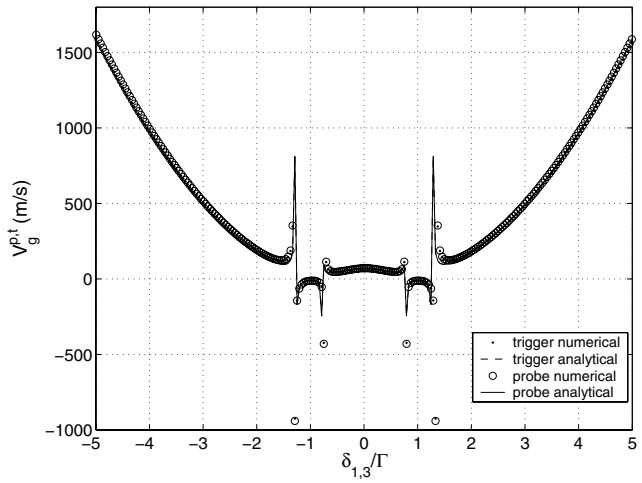

Fig. 14. Group velocity of the probe and trigger pulses versus the normalized detunings $\delta_1/\Gamma = \delta_3/\Gamma$. Lines denote the analytical predictions of equations (53) and (54) (the full line refers to the probe and the dashed line to the trigger). Circles and dots refer to the numerical solution of the OBE for the probe and trigger group velocity, respectively. Parameters correspond to the perfectly symmetric situation considered in Figure 11, that is, $\Gamma_2^{AV} = \Gamma_2 = \Gamma_4^{AV} = \Gamma_4 = \Gamma = 2\pi \times 6$ MHz, $\Omega_1 = \Omega_3 = 0.08\Gamma$, $\Omega_2 = \Omega_4 = \Gamma$, $\delta_2 = \delta_4 = 0$, $\forall i,j$ $\gamma_{ij} = \Gamma_1^{AV} = \Gamma_5^{AV} = 10^{-4}\Gamma$, and we have chosen $\mu_{32} = \mu_{34} = 10^{-29}$ C m, and $N/V = 3.0 \times 10^{13}$ cm^{-3}. Due to symmetry, one has perfect group velocity matching within a large interval of values for the detunings.

the present scheme that the condition of equal probe and trigger group velocities is automatically achieved when the corresponding parameters are equal i.e., $\mu_{32} = \mu_{34}$, $\delta_1 = \delta_3$, $\delta_2 = \delta_4$, $\Omega_2 = \Omega_4$, $\Gamma_2 = \Gamma_4$, $\gamma_{54} = \gamma_{12}$ and $\gamma_{53} = \gamma_{13}$, $\omega_1 \simeq \omega_3$. This is the main advantage of the symmetric M scheme over the asymmetric one. As we have seen above, the group velocity of a pulse is given by

$$v_g^i = \frac{c}{1 + n_g^i}, \quad i = P, T, \tag{53}$$

where the group index n_g^i is given by equation (28). The contribution of the nonlinear susceptibilities to v_g is negligible with respect to that of the linear one, which is nonzero for both probe and trigger in this case (see Eqs. (46)). Therefore, approximating χ with the linear contribution $\chi^{(1)}$ and inserting equations (47) into the definition (28), one gets the following expressions for the two group indices

$$n_g^P = \frac{N|\mu_{32}|^2}{2V\hbar\varepsilon_0}\mathrm{Re}\left\{\frac{d_1}{d_1 d_2 - |\Omega_2|^2} + \frac{\omega_1\left(d_1^2 + |\Omega_2|^2\right)}{\left(d_1 d_2 - |\Omega_2|^2\right)^2}\right\}, \tag{54a}$$

$$n_g^T = \frac{N|\mu_{34}|^2}{2V\hbar\varepsilon_0}\mathrm{Re}\left\{\frac{d_5}{d_5 d_4 - |\Omega_4|^2} + \frac{\omega_3\left(d_5^2 + |\Omega_4|^2\right)}{\left(d_5 d_4 - |\Omega_4|^2\right)^2}\right\}, \tag{54b}$$

where we have used the definitions of equations (42) for d_j, $j = 1, 2, 4, 5$. The symmetry between probe and trigger discussed above is evident also in these expressions. equations (53) and (54) are now compared with the corresponding ones obtained from the integration of the full set of Bloch equations of Appendix B. The comparison is shown in Figure 14, which refers to the completely symmetric situation between probe and trigger defined above and therefore shows exact group velocity matching for all values of the detunings $\delta_1 = \delta_3$. Figure 14 shows an excellent agreement between analytical and numerical results. The only points in which the two curves do not coincide exactly are when the detunings match the Rabi frequencies of the two pumping field. In fact in this conditions the fields are in resonance with a single atomic transition and the atoms are pumped to the excited levels. The other points that determine the disagreement are in the vicinity of the peaks. In fact in these regions the derivatives are small, because of the change in slope of the real part of the susceptibilities. Hence, the group index of equations (54) is small, and the group velocity jumps near c.

In some cases, the perfectly symmetric conditions guaranteeing group velocity matching, i.e., $\mu_{32} = \mu_{34}$, $\delta_1 = \delta_3$, $\delta_2 = \delta_4$, $\Omega_2 = \Omega_4$, $\Gamma_2 = \Gamma_4$, $\gamma_{54} = \gamma_{12}$ and $\gamma_{53} = \gamma_{13}$, are difficult to realize in practice. In fact, sometimes it may be convenient to use transitions with different Clebsch-Gordan coefficients, yielding therefore a significant discrepancy between μ_{32} and μ_{34}. The other symmetry conditions above are less problematic because

detunings and Rabi frequencies can always be made equal by the experimenter, and moreover decay and dephasing rates, even though not perfectly equal, are often comparable to each other. Just to give an example, one could implement the symmetric M scheme of Figure 10 by using the D_1 and D_2 line of the ^{87}Rb spectrum. The Zeeman sublevels $|5\mathrm{P}_{1/2}\, F = 1, m = 0\rangle$ and $|5\mathrm{P}_{3/2}\, F = 1, m = 0\rangle$ could be chosen as levels $|2\rangle$ and $|4\rangle$, respectively, while the Zeeman sublevels $|5\mathrm{S}_{1/2}\, F = 1, m = -1\rangle$, $|5\mathrm{S}_{1/2}\, F = 2, m = 1\rangle$ and $|5\mathrm{P}_{1/2}\, F = 1, m = 1\rangle$ could chosen as levels $|1\rangle$, $|3\rangle$ and $|5\rangle$, respectively (see also Ref. [14] for a similar choice). For these levels the atomic transitions related to the probe and trigger have dipole moment matrix elements μ_{32}, μ_{34} differing by a factor $\sqrt{10}$, violating therefore the symmetry condition. It is evident however that this slight asymmetry can be compensated (so that group velocity matching can be still achieved in a restricted but still useful range of detunings) by properly adjusting the Rabi frequencies of the tuner field Ω_4 and of the coupling field Ω_2, which will be no more equal. In fact, by imposing group velocity matching at the center of the transparency window, i.e., for $\delta_{12} = \delta_{34} = 0$, we derive the condition

$$\Omega_2 = \alpha \Omega_4, \tag{55}$$

where the *correction factor* α is given by

$$\alpha = \sqrt{\frac{|\mu_{32}|^2}{|\mu_{34}|^2}\frac{\omega_1}{\omega_3}}. \tag{56}$$

As shown in Figure 15, if the adjustment condition of equations (55) and (56) is taken into account, one still gets equal probe and trigger group velocities in the case of the ^{87}Rb five–level scheme specified above, at least within the entire EIT window.

Finally, we note also that the problem with the pulse *propagation*, present in the asymmetric arrangement (cf. Sect. 2.5) is absent in the symmetric arrangement. This is because the dispersion, and the related group velocity reduction have its origin in the *linear* part of the susceptibility for both, probe and trigger pulses. Hence there is no apparent singularity in the trigger group velocity, which in asymmetric case stemmed from the nonlinear origin of trigger dispersion.

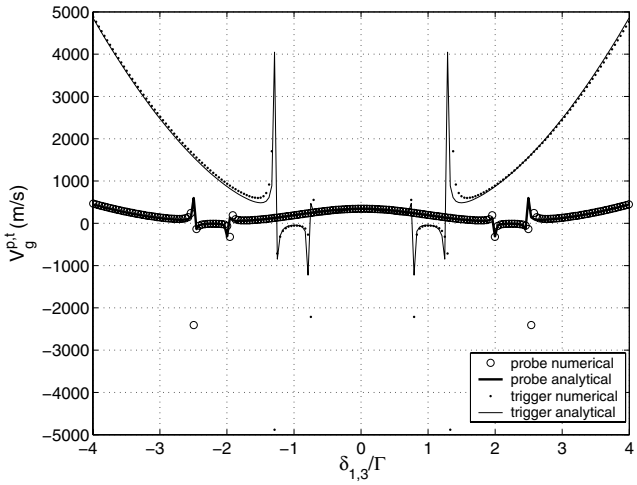

Fig. 15. Group velocity of the probe and trigger pulses versus the normalized detunings $\delta_1/\Gamma = \delta_3/\Gamma$. Full lines denote the analytical predictions of equations (53) and (54) (the thick line refers to the probe and the thin line to the trigger). Circles and dots refer to the numerical solution of the OBE for the probe and trigger group velocity, respectively. Parameters correspond to the five–level scheme derived from the D_1 and D_2 lines of the ^{87}Rb spectrum described in the text, $\Gamma_2^{AV} = \Gamma_2 \simeq 36$ MHz, $\Gamma_4^{AV} = \Gamma_4 \simeq 38$ MHz, $\mu_{32} = 1.27 \times 10^{-29}$ Cm, $\mu_{34} = 5.7 \times 10^{-30}$ Cm, $\Omega_4 = \Gamma$, $\Omega_2 = 2.22\Gamma$, $\Omega_1 = \Omega_3 = 0.08\Gamma$, $\delta_2 = \delta_4 = 0$, $\forall i, j\ \gamma_{ij} = \Gamma_1^{AV} = \Gamma_5^{AV} = 10^{-4}\Gamma$, $N/V = 3.0 \times 10^{13}$ cm^{-3}. The asymmetry between the two dipole moment matrix elements has been compensated by adjusting the value of Ω_2. In this way group velocity matching is achieved within the entire EIT window.

4 Conclusions

We have studied a five-level atomic system in two different but related M-configurations. We focused on the nonlinear properties of the system and specifically on the conditions for the optimization of the cross-phase modulation between two weak fields of interest, which we have named probe and trigger fields. Both systems have been studied from a semiclassical point of view, i.e., by describing all the fields in terms of their Rabi frequencies. We have seen that both linear and nonlinear properties are well described by an approach based on amplitude variables, which has been shown to reproduce well the numerical solution of the exact optical Bloch equations describing the system.

Both the asymmetric and the symmetric M scheme are able to provide a giant cross-Kerr modulation, which may be useful for many applications. Both M schemes can be seen as a "duplication" of the usual three-level Λ scheme at the basis of EIT, one for the probe and one for the trigger fields. In the asymmetric scheme, only the probe drives a significantly populated transition and a large cross-Kerr effect is obtained when either the probe or the trigger is slightly detuned from the two-photon resonance condition. The corresponding nonlinear phase shift, yielding for example the conditional phase shift of equation (1) of a quantum phase gate for photonic qubits, can become very large, especially when the probe and trigger group velocities, slowed down by EIT, become equal. In the asymmetric scheme, this group velocity matching can be achieved by properly adjusting the detuning and the intensity of the control field of the trigger Λ system. In the symmetric M scheme, the atomic population is equally shared by the probe and trigger transitions. Adjusting the corresponding parameters (Rabi frequencies, detunings) so that the two Λ systems become identical, probe and trigger experience the same interaction with the atomic medium and group velocity matching is achieved automatically. In this case a significant nonlinear cross-phase modulation is achieved only if both Λ schemes are slightly and equally detuned from two-photon resonance, so to remain still within the transparency window. In fact, due to EIT,

the susceptibility vanishes at all orders at the exact two-photon resonance condition.

This work has been partly supported by the European Commission through FP6/2002/IST/FETPI SCALA: 'Scalable Quantum Computing with Light and Atoms', contract No. 015714 and CONQUEST network, MRTN-CT-2003-505089.

Appendix A: Optical Bloch equations – asymmetric case

From equations (7) and (19), and using the definitions of equations (20–22), one gets the following set of equations for the atomic populations σ_{ii}

$$\dot\sigma_{11} = i\Omega_1\sigma_{21} - i\Omega_1^\star\sigma_{12} + \Gamma_{41}\sigma_{44} + \Gamma_{21}\sigma_{22}, \tag{A.1a}$$

$$\dot\sigma_{22} = -i\Omega_1\sigma_{21} + i\Omega_1^\star\sigma_{12} - i\Omega_2\sigma_{23} + i\Omega_2^\star\sigma_{32} - \Gamma_2\sigma_{22}, \tag{A.1b}$$

$$\dot\sigma_{33} = i\Omega_3\sigma_{43} - i\Omega_3^\star\sigma_{34} + i\Omega_2\sigma_{23} - i\Omega_2^\star\sigma_{32} + \Gamma_{43}\sigma_{44} + \Gamma_{23}\sigma_{22}, \tag{A.1c}$$

$$\dot\sigma_{44} = i\Omega_3^\star\sigma_{34} - i\Omega_3\sigma_{43} - i\Omega_4\sigma_{45} + i\Omega_4^\star\sigma_{54} - \Gamma_4\sigma_{44}, \tag{A.1d}$$

$$\dot\sigma_{55} = i\Omega_4\sigma_{45} - i\Omega_4^\star\sigma_{54} + \Gamma_{25}\sigma_{22} + \Gamma_{45}\sigma_{44}, \tag{A.1e}$$

and the following set of equations for the atomic coherences σ_{ij}, $i \neq j$,

$$\dot\sigma_{12} = -i\delta_1\sigma_{12} + i\Omega_1(\sigma_{22} - \sigma_{11}) - i\Omega_2\sigma_{13} - \frac{\Gamma_2 + \gamma_{12}}{2}\sigma_{12}, \tag{A.2a}$$

$$\dot\sigma_{13} = -i\delta_{12}\sigma_{13} + i\Omega_1\sigma_{23} - i\Omega_3^\star\sigma_{14} - i\Omega_2^\star\sigma_{12} - \frac{\gamma_{13}}{2}\sigma_{13}, \tag{A.2b}$$

$$\dot\sigma_{14} = -i\delta_{13}\sigma_{14} + i\Omega_1\sigma_{24} - i\Omega_3\sigma_{13} - i\Omega_4\sigma_{15} - \frac{\gamma_{14} + \Gamma_4}{2}\sigma_{14}, \tag{A.2c}$$

$$\dot\sigma_{15} = -i\delta_{14}\sigma_{15} + i\Omega_1\sigma_{25} - i\Omega_4^\star\sigma_{14} - \frac{\gamma_{15}}{2}\sigma_{15}, \tag{A.2d}$$

$$\dot\sigma_{23} = i\delta_2\sigma_{23} + i\Omega_1^\star\sigma_{13} - i\Omega_3^\star\sigma_{24} + i\Omega_2^\star(\sigma_{33} - \sigma_{22}) - \frac{\Gamma_2 + \gamma_{23}}{2}\sigma_{23}, \tag{A.2e}$$

$$\dot\sigma_{24} = i\delta_{23}\sigma_{24} - i\Omega_3\sigma_{23} - i\Omega_4\sigma_{25} + i\Omega_2^\star\sigma_{34} + i\Omega_1^\star\sigma_{14} - \frac{\Gamma_2 + \Gamma_4 + \gamma_{24}}{2}\sigma_{24}, \tag{A.2f}$$

$$\dot\sigma_{25} = i\delta_{24}\sigma_{25} + i\Omega_1^\star\sigma_{15} + i\Omega_2^\star\sigma_{35} - i\Omega_4^\star\sigma_{24} - \frac{\Gamma_2 + \gamma_{25}}{2}\sigma_{25}, \tag{A.2g}$$

$$\dot\sigma_{34} = -i\delta_3\sigma_{34} + i\Omega_3(\sigma_{44} - \sigma_{33}) + i\Omega_2\sigma_{24} - i\Omega_4\sigma_{35} - \frac{\Gamma_4 + \gamma_{34}}{2}\sigma_{23}, \tag{A.2h}$$

$$\dot\sigma_{35} = -i\delta_{34}\sigma_{35} + i\Omega_3\sigma_{45} + i\Omega_2\sigma_{25} - i\Omega_4^\star\sigma_{34} - \frac{\gamma_{35}}{2}\sigma_{35}, \tag{A.2i}$$

$$\dot\sigma_{45} = i\delta_4\sigma_{45} + i\Omega_3^\star\sigma_{35} + i\Omega_4^\star(\sigma_{55} - \sigma_{44}) - \frac{\Gamma_4 + \gamma_{45}}{2}\sigma_{45}, \tag{A.2j}$$

where we have also defined the composite detunings $\delta_{23} = \delta_2 - \delta_3$, $\delta_{24} = \delta_2 - \delta_3 + \delta_4$, and $\delta_{34} = \delta_3 - \delta_4$.

Appendix B: Optical Bloch equations – symmetric case

From equations (40) and (19), and using the definitions of equations (20–22), one gets the following set of equations for the atomic populations σ_{ii}

$$\dot\sigma_{11} = \imath\Omega_2\sigma_{21} - \imath\Omega_2^\star\sigma_{12} + \Gamma_{41}\sigma_{44} + \Gamma_{21}\sigma_{22}, \tag{B.1a}$$

$$\dot\sigma_{22} = \imath\Omega_2\sigma_{12} - \imath\Omega_2^\star\sigma_{21} - \imath\Omega_1\sigma_{23} + \imath\Omega_1^\star\sigma_{32} - \Gamma_2\sigma_{22}, \tag{B.1b}$$

$$\dot\sigma_{33} = \imath\Omega_3\sigma_{43} - \imath\Omega_3^\star\sigma_{34} + \imath\Omega_1\sigma_{23} - \imath\Omega_1^\star\sigma_{32} + \Gamma_{43}\sigma_{44} + \Gamma_{23}\sigma_2, \tag{B.1c}$$

$$\dot\sigma_{44} = \imath\Omega_3^\star\sigma_{34} - \imath\Omega_3\sigma_{43} - \imath\Omega_4\sigma_{45} + \imath\Omega_4^\star\sigma_{54} - \Gamma_4\sigma_{44}, \tag{B.1d}$$

$$\dot\sigma_{55} = \imath\Omega_4\sigma_{45} - \imath\Omega_4^\star\sigma_{54} + \Gamma_{45}\sigma_{44} + \Gamma_{25}\sigma_{22}, \tag{B.1e}$$

while the equations for the coherences are

$$\dot\sigma_{12} = -\imath\delta_2\sigma_{12} + \imath\Omega_2(\sigma_{22} - \sigma_{11}) - \imath\Omega_1\sigma_{13} - \frac{\Gamma_2 + \gamma_{12}}{2}\sigma_{12}, \tag{B.2a}$$

$$\dot\sigma_{13} = \imath(\delta_1 - \delta_2)\sigma_{13} + \imath\Omega_2\sigma_{23} - \imath\Omega_3^\star\sigma_{14} - \imath\Omega_1^\star\sigma_{12} - \frac{\gamma_{13}}{2}\sigma_{13}, \tag{B.2b}$$

$$\dot\sigma_{14} = \imath(\delta_1 - \delta_2 - \delta_3)\sigma_{14} + \imath\Omega_2^\star\sigma_{24} - \imath\Omega_3\sigma_{13} - \imath\Omega_4\sigma_{15} - \frac{\Gamma_4 + \gamma_{14}}{2}\sigma_{14}, \tag{B.2c}$$

$$\dot\sigma_{15} = \imath(\delta_1 - \delta_2 - \delta_3 + \delta_4)\sigma_{15} + \imath\Omega_2^\star\sigma_{25} - \imath\Omega_4^\star\sigma_{14} - \frac{\gamma_{15}}{2}\sigma_{15}, \tag{B.2d}$$

$$\dot\sigma_{23} = \imath\delta_1\sigma_{23} + \imath\Omega_2^\star\sigma_{13} - \imath\Omega_3^\star\sigma_{24} + \imath\Omega_1^\star(\sigma_{33} - \sigma_{22}) - \frac{\Gamma_2 + \gamma_{23}}{2}\sigma_{23}, \tag{B.2e}$$

$$\dot\sigma_{24} = \imath(\delta_1 - \delta_3)\sigma_{24} - \imath\Omega_3\sigma_{23} - \imath\Omega_4\sigma_{25} + \imath\Omega_2^\star\sigma_{14} + \imath\Omega_1^\star\sigma_{34} - \frac{\Gamma_2 + \Gamma_4 + \gamma_{24}}{2}\sigma_{24}, \tag{B.2f}$$

$$\dot\sigma_{25} = \imath(\delta_1 + \delta_4 - \delta_3)\sigma_{25} + \imath\Omega_2\sigma_{15} + \imath\Omega_1^\star\sigma_{35} - \imath\Omega_4^\star\sigma_{24} - \frac{\Gamma_2 + \gamma_{25}}{2}\sigma_{25}, \tag{B.2g}$$

$$\dot\sigma_{34} = -\imath\delta_3\sigma_{34} + \imath\Omega_1\sigma_{24} - \imath\Omega_4\sigma_{35} + \imath\Omega_3(\sigma_{44} - \sigma_{33}) - \frac{\Gamma_4 + \gamma_{34}}{2}\sigma_{34}, \tag{B.2h}$$

$$\dot\sigma_{35} = -\imath(\delta_3 - \delta_4)\sigma_{35} - \imath\Omega_3\sigma_{45} + \imath\Omega_1\sigma_{25} - \imath\Omega_4^\star\sigma_{34} - \frac{\gamma_{35}}{2}\sigma_{35}, \tag{B.2i}$$

$$\dot\sigma_{45} = \imath\delta_4\sigma_{45} + \imath\Omega_4^\star(\sigma_{55} - \sigma_{44}) + \imath\Omega_3^\star\sigma_{35} - \frac{\Gamma_4 + \gamma_{45}}{2}\sigma_{45}. \tag{B.2j}$$

References

1. H. Schmidt, A. Imamoğlu, Opt. Lett. **23**, 1007 (1998)
2. R.W. Boyd, *Nonlinear Optics* (Academic, San Diego, Calif., 1992)
3. A. Sinatra, J.F. Roch, K. Vigneron, Ph. Grelu, J.-Ph. Poizat, K. Wang, P. Grangier, Phys. Rev. A **57**, 2980 (1998); J.-F. Roch, K. Vigneron, Ph. Grelu, A. Sinatra, J.-Ph. Poizat, Ph. Grangier, Phys. Rev. Lett. **78**, 634 (1997)
4. M.A. Nielsen, I.L. Chuang, *Quantum Computation and Quantum Information* (Cambridge University Press, Cambridge 2000)
5. H. Schmidt, A. Imamoğlu, Opt. Lett. **21**, 1936 (1996)
6. E. Arimondo, in *Progress in Optics* XXXV, edited by E. Wolf (Elsevier, Amsterdam, 1996)
7. S.E. Harris, Phys. Today **50**, 36 (1997); M.O. Scully, M.S. Zubairy, *Quantum Optics* (Cambridge University Press, Cambridge, UK, 1997)
8. M. Fleischhauer, A. Imamoğlu, J. Marangos, Rev. Mod. Phys. **77**, 633 (2005)
9. M.D. Lukin, A. Imamoğlu, Nature **413**, 273 (2001) and references therein
10. S.E. Harris, L.V. Hau, Phys. Rev. Lett. **82**, 4611 (1999)
11. L.V. Hau, S.E. Harris, Z. Dutton, C.H. Berhoozi, Nature **397**, 594 (1999); M.M. Kash, V.A. Sautenkov, A.S. Zibrov, L. Hollberg, G.R. Welch, M.D. Lukin, Y. Rostovtsev, E.S. Fry, M.O. Scully, Phys. Rev. Lett. **82**, 5229 (1999)
12. D.F. Phillips, A. Fleischhauer, A. Mair, R.L. Walsworth, M.D. Lukin, Phys. Rev. Lett. **86**, 783 (2001)
13. H. Kang, Y. Zhu, Phys. Rev. lett. **91**, 093601 (2003); H. Kang, G. Hernandez, Y. Zhu, Phys. Rev. Lett. **93**, 073601 (2004); H. Kang, G. Hernandez, Y. Zhu, Phys. Rev. A **70**, 061804 (2004); H. Kang, G. Hernandez, Y. Zhu, Phys. Rev. A **70**, 011801 (2004); H. Wang, D. Goorskey, M. Xiao, Phys. Rev. Lett. **87**, 073601 (2001)
14. C. Ottaviani, D. Vitali, M. Artoni, F. Cataliotti, P. Tombesi, Phys. Rev. Lett. **90**, 197902 (2003)
15. S. Rebić, D. Vitali, C. Ottaviani, P. Tombesi, M. Artoni, F. Cataliotti, R. Corbalàn, Phys. Rev. A **70**, 032317 (2004); D. Petrosyan, Y.P. Malakyan, Phys. Rev. A **70**, 023822 (2004)
16. D. Petrosyan, G. Kurizki, Phys. Rev. A **65**, 033833 (2002)
17. M.S. Zubairy, A.B. Matsko, M.O. Scully, Phys. Rev. A **65**, 043804 (2002); A.B. Matsko, I. Novikova, G.R. Welch, M.S. Zubairy, Opt. Lett. **28**, 96 (2003); A.D. Greentree, D. Richards, J.A. Vaccaro, A.V. Durrant, S.R. de Echaniz, D.M. Segal, J.P. Marangos, Phys. Rev. A **67**, 023818 (2003)
18. M.D. Lukin, A. Imamoğlu, Phys. Rev. Lett. **84**, 1419 (2000)
19. D. Vitali, M. Fortunato, P. Tombesi, Phys. Rev. Lett. **85**, 445 (2000)
20. S. Lloyd, Phys. Rev. Lett. **75**, 346 (1995)
21. Q.A. Turchette, C.J. Hood, W. Lange, H. Mabuchi, H.J. Kimble, Phys. Rev. Lett. **75**, 4710 (1995)
22. C. Ottaviani, S. Rebić, D. Vitali, P. Tombesi, Phys. Rev. A **73**, 010301(R) (2006)
23. E. Knill, R. Laflamme, G.J. Milburn, Nature **409**, 46 (2001)
24. D.A. Braje, V. Balic, G.Y. Yin, S.E. Harris, Phys. Rev. A **68**, 041801 (2003); D.A. Braje, V. Balic, S. Goda, G.Y. Yin, S.E. Harris, Phys. Rev. Lett. **93**, 183601 (2004)